Seasonal Pumped Thermal Energy Storage with an 88% efficiency

The author of the study graduated at the end of the 80s from the Electrical Department of the then Helsinki University of Technology, majoring in Software Engineering. This research was carried out in 2023–2024 in my own time alongside the actual day job. All new ideas presented here are freely available to others. All references have been reviewed as of August 2024.

Introduction

Storing wind and solar energy is one of the biggest challenges of the green transition. Here is a possible solution to that problem. The electricity is stored as heat in a cone-shaped open pit dug filled with gravel. The storage has two overlapping gas tight halves insulated from each other. The mass of the upper low-pressure storage is used to pressurize the lower high-pressure storage, where the heat is stored in gravel. A two-way closed Brayton cycle is implemented between these chambers with gas turbines and compressors. In the scientific literature, the concept is abbreviated as PTES for Pumped Thermal Energy Store.

Electrical energy is loaded into the storage with the reverse Brayton cycle, which works on the same principle as the heat pump. The main compressor heats the hot gas stored in the upper part of the low-pressure storage by pressurizing it to red-hot upper part of the high-pressure storage. At the same time, the opposite cryogenic turbine keeps the storage pressures constant by cooling the cold gas from the lower part of the high-pressure storage to the dew point and saving it to the lower part of the low-pressure storage.

The discharge of electricity takes place with the usual Brayton cycle, where the red-hot gas from the high-pressure storage is discharged through the main turbine to the upper part of the low-pressure storage to wait for the next charge. The pressure difference between the storages is kept constant by compressing the gas at the dew point from the lower part of the low-pressure storage with a cryogenic compressor to the cold lower part of the high-pressure storage.

The gas discharged from the turbine and compressor flows through the gravel layers of the storages while either heating up or cooling down to the temperature of the aggregate in the upper or lower part of the storage. Thus, in this solution, the gravel functions as both a heat storage and a heat exchanger at the same time. Since the efficiency of the system cannot be 100%, extra heat accumulates during loading and unloading, which can be used as district heating or alternatively partially recycled back into the process using a larger pressure difference in the discharge. The lower pressure is adjusted so that the temperature of the gas coming out of the turbine is the same as the temperature of the gas being compressed during the charging phase. The solution simplifies the structure of the storage because the excess heat produced by the turbine does not need to be cooled and the hot compressor and turbine can share the same pipes and gas distribution channels.

The excess heat accumulated on the cold side is cooled with a separate high-power heat pump during the charging. It cools the cold gas coming from the bottom of the high-pressure storage, so that the gas coming out of the cryogenic turbine is slightly wet. The liquid gas is stored to another storage to keep the gas pressures constant. The heat produced by the cooling heat pump must be fed directly into the district heating network, stored in some other way, or cooled as waste heat.

With the search words "energy store Brayton cycle” can be found Several new scientific studies can be found on the thermal storage of electricity based on the Brayton cycle. A recently published study, *Derived energy*

storage systems from Brayton cycle[1] is an overview of the current state of research in the field. In it, the researchers compare CAES (compressed air energy system) and PTES (pumped thermal energy store) solutions on a theoretical level. For example, under the leadership of Josh McTigue, the feasibility of PTES projects has been mapped[2] [3]With funding from the US Department of Energy. The researchers considered a 75% recovery efficiency to be achievable with supercritical carbon dioxide when the heat is stored in table salt [4]. The technical economic comparison of PTES solutions has also been studied in another study [5], where it was also decided to propose different pressure ratios for charge and discharge.

Here we will present concrete solutions to the further development needs and technical-economic challenges of PTES mentioned in the studies. In this solution, the gravel acts as a massive heat storage and heat exchanger. With step-by-step active control of the tip gap and rotational velocity, the higher losses of the high-pressure stages of current turbo equipment can be eliminated, and their efficiencies can be optimized to the upper limits or partially even above them. In addition, the inexpensive rock open pit technology enables more than two orders of magnitude lower storage costs/kWh compared to current electricity storages.

In this study the working principle of the solution will be described in more detail, its operation will be studied programmatically with an analysis program, the dimensioning of the energy storage will be optimized, problems related to the technical implementation will be analyzed and possible solutions proposed.

The lower pressure to be used, the ratio of lower and high-pressure, the porosity of the gavel, the specific gravity of the gravel and the steepness of the open pit wall determine the smallest possible size of the energy storage. However, with energy storages of less than ten million gravel tons, various size-related problems and equipment costs increase rapidly. The technical upper limit for the loading and unloading power is set by the increasing flow resistance of the gravel and its heat exchange capability, which are opposite properties. The power of heat exchange is directly proportional to the surface area of the gravel, but on the other hand, the small average grain size and low porosity of the gravel increase the gas flow resistance.

Nitrogen has been chosen as the gas because it is inexpensive to produce, and its low vaporization temperature allows for a larger temperatures difference between the cold and hot cycles compared to other possible gases. In addition, nitrogen is an inert gas, meaning it reacts very weakly with other elements. Thus, it is a problem-free gas compared to hydrogen, oxygen or carbon dioxide. Finally, the unit costs of stored energy and charging and discharging power and the return on investment are evaluated. The analysis program calculates the unit costs of energy according to the given parameters.

The default parameters of the energy storage analysis program produce an energy storage with a storage capacity of 1939 GWh and a discharge capacity of 1041 MW. The unit cost of the storage capacity is 28 cents/kWh. It is currently about 1/600 of the unit cost of a lithium-ion battery. When the efficiencies of the plant's turbines and compressors are optimized as shown above to the upper limit set by current technology,

---

[1]https://www.sciencedirect.com/science/article/pii/S2589004224006813#:~:text=energy%20for%20storage.-,In%20discharge%20process%2C%20a%20Brayton%20cycle%20is%20formed%20by%20the,is%20converted%20back%20to%20electricity.

[2] https://core.ac.uk/download/pdf/42338379.pdf

[3]https://www.researchgate.net/publication/356766772_Techno-economic_analysis_of_recuperated_Joule-Brayton_pumped_thermal_energy_storage

[4] https://www.energy.gov/sites/default/files/2020/12/f81/SETO%20PTES%20Workshop%20McTigue_NREL.pdf

[5]https://www.mdpi.com/1996-1073/15/24/9595

then at best 88% of the electricity charged from the grid would be recovered as electricity, when the upper temperature of the high-pressure storage is 900 °C, and the losses of cooling heat pumps, vacuum gearboxes and generators are also included.

General operating principle and dimensions of the energy storage

The figure below shows a cross-section of the energy storage produced by the default parameters of the Analysis program. Its size, 25 million tons, corresponds to the annual extraction volume of Yara's Siilijärvi phosphate mine (around 20–30 million tons) [6]. There, the mining contractor's 200 employees are responsible for all mining, crushing, transporting the fine crushed stone to the processing unit and finally placing the waste rock. Thus, mining the energy storage in the picture, crushing, driving up, sieving and spreading it back could be a job of approximately 200 man-years, and its unit price is here estimated to be slightly higher than the average mining cost of large open pit mines of 10 euros/ton.

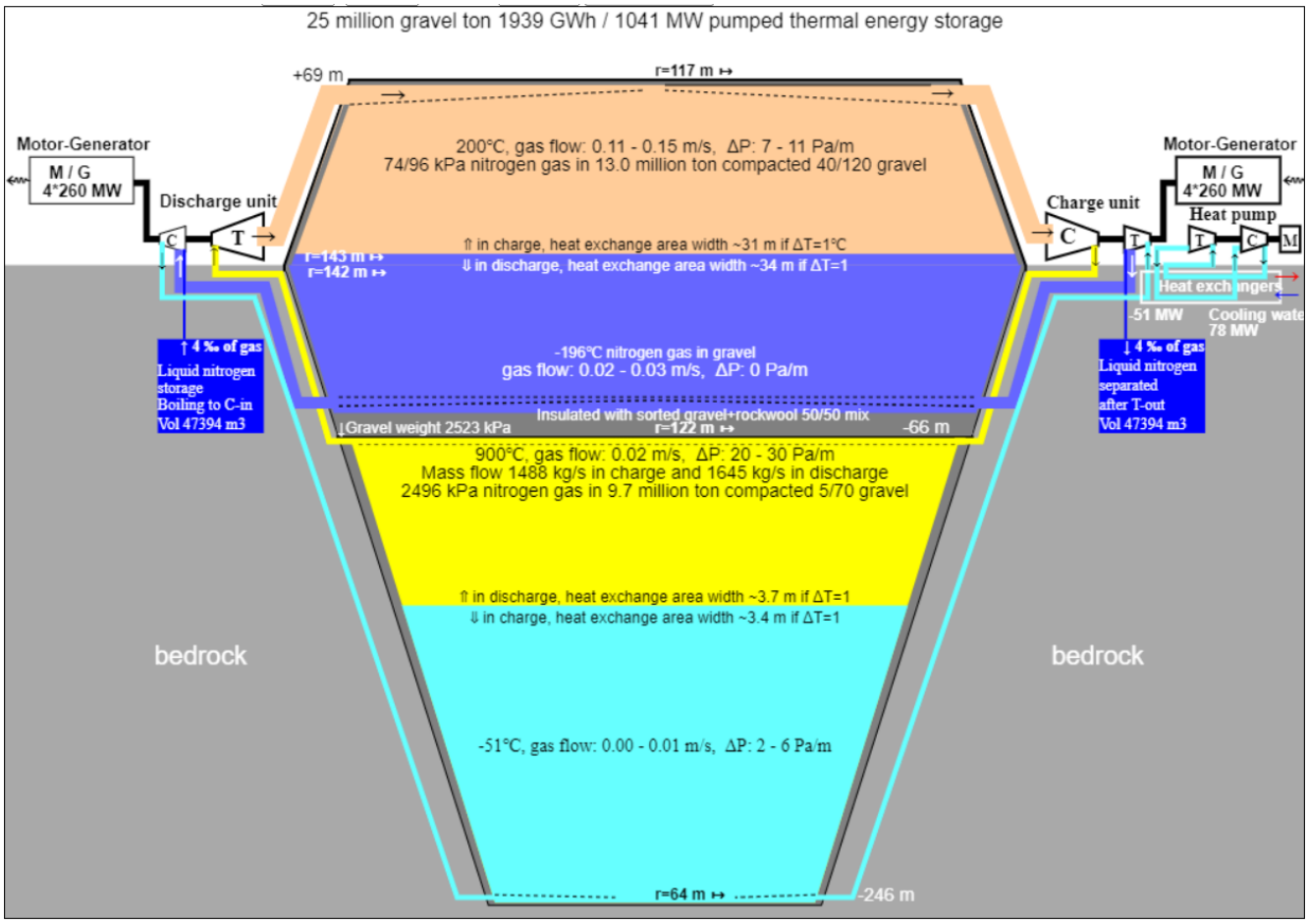

Figure 1. Cross-section of the energy storage and operating principle

In the picture, the steepness of the reinforced rock wall throughout the open pit (including ramps) is 73 degrees, the high temperature is 900 °C, the average efficiency of the compressors stages is 0.955 and the stage efficiency of the turbines is 0.97. The high-pressure of the energy storage is 2496 kPa, the lower pressure is 96 kPa in charge and 74 kPa in discharge. In this case, the return efficiency of electricity is 87.9%, when the cooling work of the cold side of 8.2%, the losses of the vacuum gearboxes 2.0% and the losses of the generators 1.9% are included. The default value for the upper temperature is 900 °C, because then the need

[6] https://www.yara.fi/tietoa-yarasta/yara-suomi/toimipaikat/siilinjarvi/tuotantolaitos/

for cooling the rotor blades operating at high pressure is still quite low, and the long-term usability of the best-suited mafic and ultramafic gravel should be good.

For the sake of clarity, charging and discharging are placed on different sides in the picture, even though they share the same generator that also acts as a motor. In the picture, the plant would consist of four identical units, so that they could be run flexibly according to the demand and supply of electricity, and so that they could be serviced one at a time. In addition, the charge and discharge powers can be somewhat adjusted by changing the pressure of the upper storage.

If necessary, the Analysis program increases the amount of excavation, so that with the given parameters, the mass of the aggregate perpendicularly above is at least the same as the pressure of the high pressure. An error tolerance of 100 kPa (ie about one atmosphere) is left as the default value. The amount of aggregate used to store heat and cold in the upper low-pressure tank is about 30% greater than in the high-pressure storage, because the specific heat capacity of the aggregate increases by more than 60% when the temperature rises from room temperature to 550 °C, and then increases slowly until it starts to rise again faster near the melting point of the aggregate.

In the picture, black lines are gas tight boundaries, which may be steel, or aluminum plates welded together, injected rock, or even frozen rock. Pumping caused by the thermal expansion and contraction of the aggregate may gradually spread the part above the ground several meters, so the steel plate must have vertical flexible folds. At the upper temperature of the high-pressure storage, the steel plate above it turns into a soft surface that stretches and shrinks along with the surrounding gravel. The gas tightness of the high-pressure storage can be ensured by a mixture of fine crushed rock bearing the steel plate surface on top and crushed rock that partially melts at the temperature of the high-pressure storage, which in the heat and pressure is compressed into a solid, elastic, gas-impermeable layer.

The dark gray areas inside the black lines are thermal insulation layers with equal volumes of stone wool or biochar and a very uniform gravel with a compacted porosity of about 0.5 and a thermal conductivity 0.1 W/mK. The convection of heat can be minimized by adding thin horizontal layers of compacted clay. Biochar is excellent for high-temperature insulation in oxygen-free conditions. Biochar's melting point is 3000 Kelvin and thermal conductivity 0.03 W/m*K. Its pore size is very small, at best only a few micrometers [7], so it insulates thermal radiation at least one order of magnitude better than the commercial insulation products, whose cell size is at best 100– 200 micrometers. Biochar can be replaced by loose stone wool.

In the picture, the thickness of the insulation layers has been calculated so that the heat leakage is everywhere approximately 20 W/m^2. The total heat leakage from the energy storage would be less than 4 MW when fully charged. The sloping walls of the upper part above ground are also insulated from the inside with a biochar-gravel mix. The roof of the storage can be built as a hall roof, and insulated from the top stone wool, if it turns out to be a more affordable structure than a steel-coated gravel mixed with stone wool or biochar.

The gas coming from and to the pipes is distributed evenly along the channels running in the gravel so that its flow rate slows down enough so that stone dust is not carried into the equipment with the incoming gas. The gas duct in the hot upper part of the high-pressure storage are vaulted structures made of masonry or cast firebrick. The vault structures of the other three gas distribution ducts can be cast from reinforced concrete, where the steel mainly acts as concrete shrinkage reinforcement. The compressive strength of concrete

[7] https://www.energiatalous.fi/?p=2483

increases as the temperature decreases, so it is therefore perfectly suited for vault structures in very cold lower parts. The branching distribution ducts are vaults open from the bottom, below which there is a gas distribution layer about 1–2 meters thick made of washed, sorted, coarser gravel, where the gas spreads and slows down to the final flow rate.

Between the hot and cold gravel layers is a heat exchange layer a few meters high. Its height depends on the gas flow rate, density and the sieve spacing of the gravel. A small average particle size increases the surface area and thus improves heat exchange. In addition, heat conduction by radiation decreases linearly as the average particle size of the gravel decreases, so a finer gravel is used in the high-pressure vessel. On the other hand, the gas flow resistance increases very quickly as the gravel subsection decreases, so the default value 5/70 suggested by the analysis program for the high-pressure storage gravel is a considered compromise in terms of the gravel density, the height of the heat exchange zone and the gas flow resistance. The gas flow resistance calculation used is described in more detail in the description of the Analysis program.

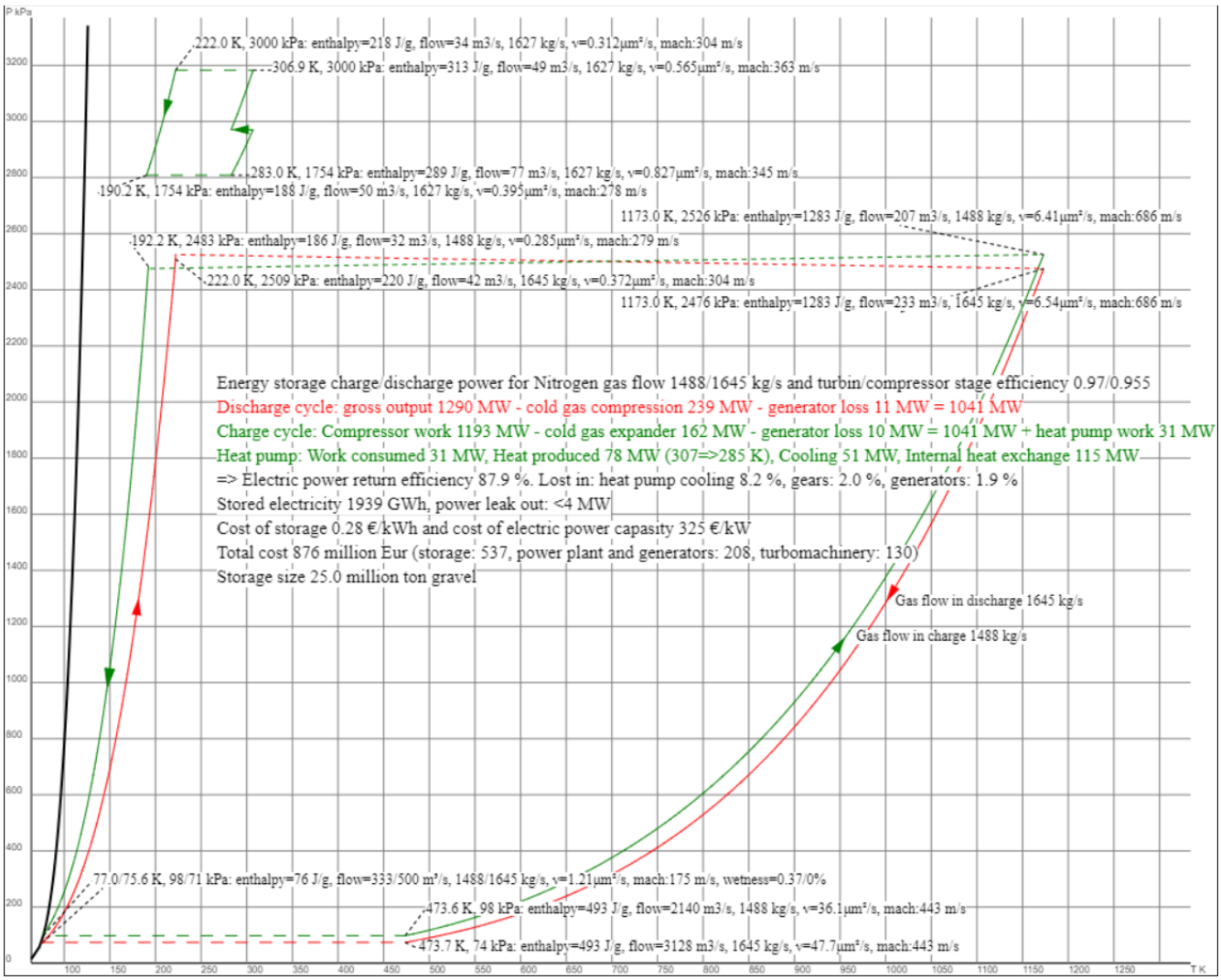

Figure 2. Operation of the energy storage as a TP diagram, with temperature in Kelvin on the horizontal axis and pressure in kilo-Pascals on the vertical axis.

Figure 2 above shows the temperature/pressure diagram drawn by the analysis program describing the operation of the plant. In it, the storage charge cycle is drawn in green and the discharge cycle in red. On compressors, the arrows pointing to the direction of gas flow are upwards and on turbines downwards. The dashed lines represent the passage of the gas through the gravel. They are slightly tilted in the direction of gas flow due to the drop in pressure caused by the gravel. The TP curves of turbines and compressors are curved, because the pressure increase, or decrease has been calculated in very small steps according to the stage efficiency. Discharge and charge cycle share the same generator, so their mass flows and equipment powers are adapted accordingly. In the center of the picture are the powers or losses of the main components, the discharge efficiency and the plant and unit price estimates calculated according to the given parameters.

Construction technology and aggregate behavior under pressure and high temperatures

Several problems must be solved in energy storage sizing and construction. The thermal expansion and contraction of the aggregate must not tear the pressure insulation of the storage or the pipe connections coming from the rock wall. The slow compaction above ground expansion and of the gravel caused by repeated heating and cooling must not hinder the operation of the plant during its planned service life.

Hot high-pressure storage aggregate

The aggregate of the high-pressure storage should withstand at least several tens of very slow heating and cooling between the upper and lower temperatures of the high-pressure storage, and at the same time maintain sufficient compressive strength so that the aggregate does not compress too much. In addition, the aggregate should not evaporate gases, such as sulfur, which may hinder the operation of the hot turbine. The higher-than-usual density and specific heat capacity of the aggregate are also an advantage. The most common types of mixed igneous rock found on the surface, such as granite or gneiss, do not meet these requirements. For example, granite gradually begins to lose compressive strength after exceeding a temperature of 572 °C, because then the prevailing α-crystal structure of quartz changes to a β-crystal structure that is about 4% larger in volume. This causes microcracks in the stone [8]even if the stone heats up very slowly. Probably because the volume change does not occur in the other main mineral of granite, potash feldspar, so internal stresses are created in the stone.

In the study *High Temperature Versus Geomechanical Parameters of Selected Rocks – The Present State of Research*[9], it was found that the compressive strength of sandstones and mudstones initially increased significantly up to 400 °C and then slowly began to decrease. The original 150 MPa compressive strength of a fine-grained and denser sandstone was bypassed at 1000 °C, but a coarse-grained sandstone had lost its original 60 MPa compressive strength after 800 °C. With the other tested rock types (granite, marble, and limestone), the compressive strength decreased continuously as the temperature increased, and at high temperatures it was significantly worse than the compressive strength of sandstones. Also in this study, the collapse of the compressive strength of granite was found before the temperature of 600 °C. The researchers' conclusion was that the temperature behavior of the stone's strength depends especially on its mineral composition, the size of the grains and the porosity of the stone.

In the study *Effect of heat on the mechanical properties of selected rock types in a laboratory study*[10] compared the behavior of the strength properties of diabase, granite and two quartzite slates at high temperatures. What is interesting in that study is the almost complete disappearance of the compressive strength of granite at a temperature of 1100 °C. The reason is probably the melting of potash feldspar. In that study, diabase retained its original compressive strength the best in the comparison.

---

[8] Frontiers | Fractal Characteristics and Energy Dissipation of Granite After High-Temperature Treatment Based on SHPB Experiment (frontiersin.org)

[9] https://www.academia.edu/93970453/Effect_of_heat_on_the_mechanical_properties_of_selected_rock_types_a_laboratory_study

[10] https://www.academia.edu/93970453/Effect_of_heat_on_the_mechanical_properties_of_selected_rock_types_a_laboratory_study

The same conclusion has also been reached in tests of Finnish sauna stove stones [11]. Nowadays, stove stones sold in Finland are mostly olivine gabbro (its trade name is Olivinediabase). Olivine gabbro and other stove stones can withstand a temperature of at least 1100 °C. All sauna stove stones are mafic or ultramafic rocks, i.e. they have solidified at the bottom of ancient volcanoes' eruption channels and magma chambers. You can find a general description of the formation mechanism of igneous rocks on the page https://www.geologia.fi/2018/10/24/mita-ovat-magmakivet/ , from which the Bowen reaction series in Figure 3 is copied. The image next to it of the classification of igneous rock species is copied from Wikipedia [12].

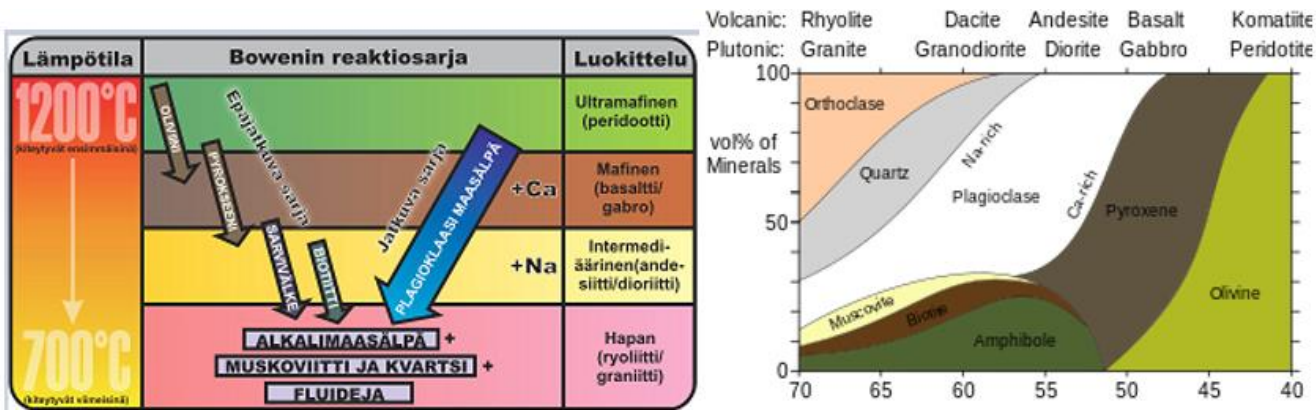

Figure 3. On the left, the Bowening reaction series, on the right, the classification of rock types according to the content of silica and sub-minerals

The mafic and ultramafic rocks also vary. On the left, Bowen's reaction series divides igneous rock types into main categories according to the crystallization temperature of magma eruptions. On the right, they are classified according to the silica content. The upper limit of the silicon dioxide (SiO_2) content of mafic rocks is 52% and 45% of ultramafic rocks. In the picture, the proportions of the main minerals of each rock type are on a vertical line. Apart from pure quartz, the heat resistance of stones generally increases as the proportion of silica decreases. For pure mafic rocks, it is about 1100 °C at 52%. The sintering temperature of pure magnesium olivine or chromite used as casting sand is about 1800 °C [13]. Mafic rock types are characterized by a dark color, alkalinity, higher density than surface rock types, and thus a higher volume specific heat capacity.

In the more precise QFPA classification,[14] rock types are classified based on the mutual sliding percentages of the four main minerals, and ultramafic rocks separately [15]based on the three main minerals. Thus, the properties and melting points of so-called pure rock types also depend on the mineral contents and other impurities. Each mineral of a stone first softens and finally melts in their own temperature range. When its minerals start to soften the compressive strength of the stone also begins to decrease quickly, even if it is externally intact.

---

[11] https://saunologia.fi/kiuaskivet/

[12]https://en.wikipedia.org/wiki/Igneous_rock
[13] https://tupa.gtk.fi/raportti/arkisto/m19_3132_81_80.pdf
[14] https://en.wikipedia.org/wiki/QAPF_diagram
[15] https://en.wikipedia.org/wiki/Ultramafic_rock

Of the minerals, chromite and olivine and mafic plagioclase and pyroxene have high melting points. Plagioclase[16] consists of two and pyroxene[17] five different sub-minerals, with mafic minerals with a higher melting point at one end and felsic minerals with a lower melting temperature at the other end. In summary, especially alkaline subtypes of magnesium- and calcium-rich minerals have high melting points, while rocks containing potassium or sodium, respectively, melt at lower temperatures. The replacement of magnesium with iron also lowers the melting temperature of the mineral.

Not all mafic rocks can withstand high temperatures. In the absract[18] of the article *Damage and Changes in Mechanical Properties of a Gabbro Thermally Loaded up to 1,000°C*, it is stated that microcracks caused by the different thermal expansion coefficients of its mineral crystals already appeared in the gabbro sample below 600°C, and above that a significant oxidation of free iron and magnesium began. The compressive strength of the gabbro decreased dramatically in this test. The cause of the microcracks could be the high quartz content of the sample. Furthermore, no oxidation can occur in the nitrogen gas of the storage.

Finland's largest sauna stove stone quarry is in Luvia [19], which belongs to the area of diabase veins in southern Satakunta. Sauna stove rocks such as olivine diabase and peridotite serpentine have been mined from the Kemi intrusion. Very dark diabase and gabbro, sold under the trade name black granite, are mined at several stone quarries in central and eastern Finland. Mäntyharju has the only known deposit of pure [20]olivine in Finland, from which sauna stones is also mined. The melting temperature of that pure olivine has been measured at the Technical University of Helsinki at 1350 °C [21]. The mafic calcium-rich subtype of hornblende (Amphibolite[22]) also withstands high temperatures and is considered a good stove stone. Mafic hornblende has previously been mined in Hyvinkää for stove stone.

The amount of waste stone is usually quite high in most stone quarries of mafic stones. For example, at Luvia, only about 25% of the quarried stone can be sold as sauna stone. In natural stone quarries, parent stones of several cubes are cut from the rock, so the waste percentage of mafic stones is even higher [23]. The loss percentage is high, because the mafic deposits are layered and/or striated, partially, or completely metamorphosed and may be mixed with other mafic or intermediate deposits such as diorite. One typical mafic so-called waste rock is peridotite, which, however, may have even better properties than pure diabase or gabbro. Thus, mixed mafic clasts may be as useful as pure clasts of one rock type.

Finland's mafic rock deposits are quite well studied and drilled, so based on the existing research data, it is possible to focus further research on the most promising areas. In the general description of the bedrock https://tupa.gtk.fi/raportti/arkisto/50_2017.pdf the largest mafic rock areas are marked , but in the more detailed high-resolution description of the bedrock https://tupa.gtk.fi/kartta/erikoiskartta/ek_098_300dpi.pdf you can see, that smaller mafic rock areas and lines with a diameter or length of a few kilometers can be found

---

[16]https://en.wikipedia.org/wiki/Plagioclase
[17]https://en.wikipedia.org/wiki/Pyroxene
[18] https://ui.adsabs.harvard.edu/abs/2010PApGe.167.1511K/abstract
[19] https://saunologia.fi/saunagranit-luvian-kiuaskivitehatalla/

[20] https://tupa.gtk.fi/raportti/arkisto/m19_3132_81_80.pdf
[21] https://suomenkiuaskivi.fi/oliviini-kiuaskivet/
[22] https://en.wikipedia.org/wiki/Amphibolite
[23] https://www.suomalainenkivi.fi/vanha/wp-content/uploads/2016/03/luonnonkiviväkteiden_suunnentilohje_osa2.pdf

practically everywhere in Finland. The situation must be the same wherever there are old worn-out volcanoes on the earth's surface. In Europe, they can also be found outside the actual active volcanic zones, for example in England, central Germany, and central France.

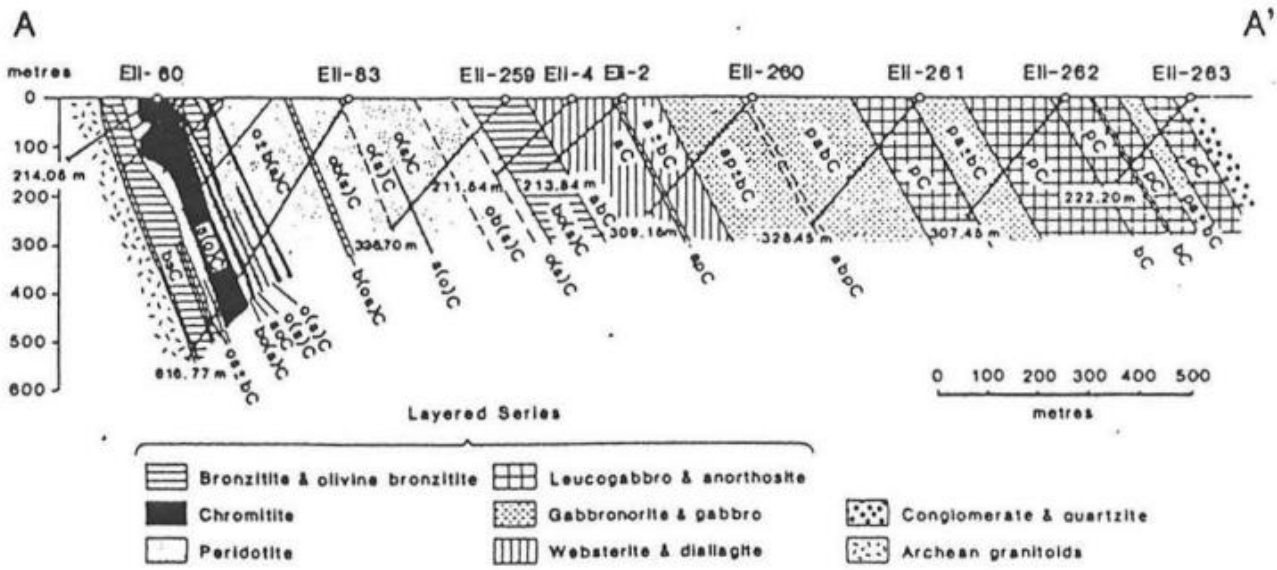

Kuva 4. Läpileikkaus A-A′ Kemin intruusiosta perustuen kairausprofiileihin. (Alapieti *et al* 1989)

The Kemi intrusion is a good example of the geology of an ultramafic deposit. There is a good description of it in Alan Forsman's Master's treatise [24], from which the picture above is copied. The picture shows a cross-section of the intrusion seen from the northeast. As a result of subsequent folding, the intrusion has tilted at an angle of 70 degrees into the earth to the northwest, and the igneous rock types separated from each other at the bottom of the magma chamber are in order from left to right, so that first there is a strip less than a kilometer wide of ultramafic magma chamber bottom minerals such as peridotite, olivine , chromite and pyroxene , so that the proportion of pyroxene increases as you go right. After that comes a well over kilometer wide strip of mafic gabbro-like rock types, which are gradually replaced on the upper surface of the intrusion by intermediate with leucogabbro and anorthosite. At the top and bottom of the intrusion, silicates have undergone metamorphosis and changed to serpentine, chlorite, amphibole, talc, and carbonates. Thus, in terms of energy storage, the most important properties of the aggregate, i.e. high melting point, low thermal corrosion, vary, but probably the best aggregate can be found in the partially metamorphosed part of the left edge from the ultramafic zone. There used to be a stove stone quarry right there. Also, the untransformed gabbro zone in the middle could be a promising location for energy storage. Located at the mouth of Kemijoki, the Kemi intrusion and Luvia are located close to the hubs of the Finnish electricity grid, so electricity could be charged and discharged from several directions.

Some mafic and ultramafic rock deposits may contain rocks with asbestos fibers. However, the minor asbesto content has not been found to be a significant problem in the utilization of those deposits[25].

The previously referred study, which compared the strength properties of four rock types after the heating to 1100 °C, also two schists retained their original strength reasonably well. This was probably due to their low

[24] https://saunologia.b-cdn.net/wp-content/uploads/2018/02/1997-Forsman-kiuaskivet_silikaattimineraalit-SaunologiaS.pdf
[25] https://tupa.gtk.fi/julkaisu/tutkimusraportti/tr_127.pdf

feldspar content (4%) and quite high quartz content. The melting point of pure quartzite is over 1700 °C, but 1400 °C is probably the highest operating temperature for quartzite in practice, because above it is the next significant change in the crystal structure and volume of quartz. In Finland, pure quartzite deposits can be found at least in Lapland. In Finland, quartzite slate has been mined not only in Lapland but also in Nilsiä and Orivesi. In addition to pure ultramafic sands, quartz sand is also used in casting molds due to its affordability, and in them it has been learned to control its stepwise thermal expansion with iron oxides.[26]

Gravel strength requirements

The gravel starts to compress when the compressive strength of its point load is exceeded. The compressive strength of the point load test is generally considered to be 5% of the compressive strength of intact stone [27], i.e. if the compressive strength of the aggregate is 200 MPa, then its maximum point load is 10 MPa. According to the sources mentioned above, after repeated heating and cooling cycles, the compressive strength may drop to about half, i.e. 5 MPa. Since the pressure of the hot high-pressure reservoir is only slightly lower than the mass above it, only the density and height of the gravel inside its pressurized area need to be considered. If the density of the gravel is 2.34 (3.0*0.78), then the pressure increases by 2.34 MPa/100 m. Thus, if the compressive strength of the best mafic or ultramafic rock material were 200 MPa, the maximum height of the high-pressure reservoir would be about 200 meters. In practice, the compression between the side walls caused by the thermal expansion of the aggregate reduces at least somewhat the maximum possible depth of the storage. In Figure 1, the height of the high-pressure storage is 180 meters. Exceeding the maximum permissible point load is not a problem for the operation of the energy storage, if the aggregate reaches a new equilibrium state during compaction before its gas permeability drops significantly.

The heat-resistant gravel of the high-pressure storage and its insulating layers accounts for approximately 45% of the total amount of mining, so the less heat-resistant felsic and intermediate mixed crushed stone from the open pit can be placed in the upper low-pressure storage. At its bottom, the compression of the aggregate is 2.5 MPa, so the compressive strength of the aggregate used there is sufficient to be 50 MPa. In addition, the weakest aggregate can be placed at the top of the low-pressure storage. At the operating temperatures of the low-pressure storage, the aggregate does not lose its original compressive strength.

Pressurization of heat reservoirs and control of thermal expansion of the gravel

The above-ground part of the storage is pressure-insulated with a stainless-steel sheet surface welded together outside the mixed gravel and stone wool. The space between the upper and lower pressure tanks can be pressure-insulated with ordinary steel. However, the long-term thermal expansion and compaction of the above ground storage's aggregate must be taken into account in the design implementation of steel surfaces.

The coefficient of thermal expansion of basalt, gabbro and diabase is reported as $5.4 \pm 1\ 10^{-6}$ m/K [28], so the change in the volume of aggregate in the high-pressure storage caused by a temperature difference of 950 °C would be approximately 1.6%. Since the rock surrounding the storage is not flexible, the thermal expansion of the gravel takes place upwards, so the upper part of the storage could rise 2 meters when the storage is fully charged. However, part of the thermal expansion only compacts the gravel. An example of this is fire bricks, whose coefficient of thermal expansion, either due to their clay quality or porous structure, is about 30% lower than that of ordinary solid bricks. The porosity of the compacted gravel is significantly larger than the porosity

[26] https://cdn.ymaws.com/www.sand.org/resource/resmgr/docs/Research/Thiel_Paper.pdf
[27] https://www.doria.fi/bitstream/handle/10024/121669/lts_2015-68_978-952-317-181-7.pdf?sequence=1&isAllowed=y
[28] https://www.britannica.com/science/rock-geology/Thermal-properties

of the firebricks, so it can be assumed that its coefficient of thermal expansion of the gravel would also be lower than the coefficient of thermal expansion of its rock. The difference probably depends not only on the porosity of the gravel, but also on the pressure, the elasticity of the aggregate, the size of the fraction and the settings of the crusher, so the actual coefficient of thermal expansion of the gravel must be measured on a case-by-case basis under realistic pressure.

The pipes from the compressors and turbines are attached to the rock, so there must be free movement between the pipes and the gas distribution channels in the gravel. The connection between pipes and storage may also fall down several meters if the gravel of the high-pressure storage compacts over time. Thus, the connecting pipe must be very flexible and there must be a free space of several meters in the rock, that allows the possible up and down movement of the insulation layer.

In the design of the insulation layer of the high-pressure storage, its internal movement friction should also be taken into account in relation to the friction of the actual storage gravel. If the internal friction of the insulation is significantly lower than the friction of the storage gravel, the thermal expansion and contraction of the storage gravel may gradually pump the insulation gravel up. When pressed, round-edged sand sifted from a dry gravel pit slides between the fingers much easier than angular rock ash passed through the same sieve gap. Movement friction in the compression of the gravel therefore presumably depends on both the particle size and the average angularity and aspect ratio of the particles.

Thermal expansion also raises and lowers the low-pressure reservoir, but significantly less, because there the volume change of the high-pressure reservoir is distributed more widely, and its thermal movement is also smaller and opposite to the high-pressure reservoir. The difference between the upper and lower temperatures of the low-pressure storage is about 400°C, and in its upper part, two-thirds of the expansion takes place to the side. As a result of the opposite thermal movement of the storages, the main part of the thermal expansion of the low-pressure storage occurs from below, but despite this, the thermal expansion to the side in the part above the ground of the storage must be taken into account in the design. The radius of above-ground storage is 130 meters on average, and the coefficient of thermal expansion of an ordinary granite gravel is on average $7 * 10^{-6}$ m/K, so a temperature change between -196°C and 200°C could push the sidewall gravel outwards by up to 36 cm. When this is repeated, for example, 50 times, the above-ground part of the storage could gradually spread almost 18 meters, and at the same time the above-ground part would be lowered several meters, which would force the pressure of the high-pressure storage to decrease. However, such a big change would require the gravel to have a uniform contact surface to the side, and this contact surface would also be preserved when the gravel cools down. However, this is not likely because it is an almost perennial energy store, i.e. the gravel is charged and discharged maybe twice a year, and a significant part of the gravel has no contact with the adjacent stone. In addition, the middle part of the low-pressure reservoir sinks down because the upper-pressure reservoir cools below it. The above-ground part of the low-pressure reservoir could potentially widen outwards by an average of perhaps 20-40 centimeters per year during the first few decades. There is probably no need to do anything about it if the widening is initially taken into account in the structural design of the storage. Collapsing of steep side walls can be prevented by the flexible steel surface, also by horizontally placed reinforcement nets in the edge gap, and by using rougher stone on the edges. In addition, air pressure compresses the walls of the low-pressure storage inward, especially during the unloading phase, when thermal motion pushes the gravel outward. Possible support structures must be of high-grade cold-resistant austenitic steel, which does not become brittle at the dew point of nitrogen gas.

The widening of the low-pressure storage could be prevented by extending the cone excavated into the rock a few meters above the earth's surface. In this case, the gravel spread by the thermal expansion would return to its original shape when it shrinks. In addition, the gradual compaction of the lower high-pressure storage would compensate for the gradual spreading of the low-pressure storage.

The outer steel surface of the above-ground part does not tear when the storage expands if it has vertical folds of a few centimeters per meter. In a fully loaded state, the storage may be a meter higher and later descend as the aggregate compacts and the above-ground part widens, so between the vertical walls and the uniform steel surface of the roof, there must be either a two-way stretching rubber mat reinforced with steel springs or a two-way flexible steel accordion joint. The steel shell of the above-ground storage could be a two-layer flexible structure. In this case, there would be, for example, airtight concrete bricks between the steel sheets, which are attached to each other and to the steel sheets with airtight and flexible bitumen or technical rubber. In the horizontal direction, the tensile strength could be improved with flexible fibers. In addition, the structure can be strengthened with an external earth embankment.

The gas seal above the hot high-pressure storage can be made of soft, very low-carbon steel, which becomes flexible at the operating temperature of the high-pressure storage, and thus adapts to the thermal movement of the gravel. The central part of the high-pressure storage may bulge a few tens of centimeters at most in relation to its peripheral part, but compared to the surrounding bedrock, the aggregate of the storage can rise two meters. In the insulating layer of the edge, when the temperature drops, the steel can first be changed to an aluminum alloy, then to a mixture of pure aluminum and load-bearing gravel, and when the temperature drops below 200 °C near the rock, to an airtight mixture of gravel and bitumen or technical rubber fused together. At best, the long-term maximum operating temperature of heat-resistant technical rubbers is slightly over 200 °C. At that temperature, pure aluminum is probably still malleable enough, so by changing the material, the pressure insulation can be extended to the rock surface. The softness of steel and aluminum depends on their additives such as carbon or silicon and heat treatment. The toughness of the soft insulation layers can be improved by mixing them with, for example, carbon fiber fibers, and their compressive strength can be improved by mixing them with a good-quality gravel of equal size, which prevents the soft pressure insulation from moving laterally. Above and below the insulation layer, the gravel must be fine enough so that the soft metal or rubber is not squeezed uncontrollably inside the gravel. In the case of pressure insulation, the rock wall is perpendicular and covered with steel, so that the contact between the rock and the insulation layer would be as gas tight and would slide along with the gravel in the vertical direction.

The gas seal of the steel surface above the high-pressure storage can be secured with a very compact layer of gravel and biotite. Biotite becomes plastic and partially melts at the operating temperature. Biotite-containing minerals starts to melt at about 800 °C[29]. The permeability of a meter-thick backup layer may at best be even lower than a steel plate of a few millimeters [30]. Under compression and heat, the mixture is likely to become completely gas impermeable if at least 20% of its minerals either melt or become plastic, completely filling the porosity of the compacted gravel.

The cracks and surfaces of the storage's rock walls can be sprayed with concrete to make them gas tight. At the same time, it enables steep rock cutting and improves work safety. In highly fractured areas, a single steel plate

---

[29] https://www.researchgate.net/publication/259049396_Experimental_melting_of_biotite_plagioclase_quartz_muscovite_assemblages_and_implications_for_crustal_melting

[30] Ranges of common intrinsic permeabilities https://en.wikipedia.org/wiki/Permeability_(materials_science)

anchored to the rock can be left inside the spray concrete. The rock can also be strengthened and made gas tight by freezing it below the groundwater level. This may also have to be done if the storage is penetrated by an active rock expansion joint that cannot be concreted to be gas tight with certainty. Freezing is used to strengthen rock in rock construction. Above, the thickness of the insulation has been defined so that the continuous heat loss of a full storage is 7 MW. Of that, maybe about 4 MW seeps into the rock. When the cooling power of the rock pipeline is sized sufficiently large, freezing of the rock could be done in Finland in winter almost free of charge. Continuous freezing with a heat pump would require less than 1 MW power, since the average temperature difference would probably be less than 20 °C.

Energy storage simulation and analysis program

The energy storage simulation and analysis program is a browser-based research and design aid built on top of the JavaScript adaptation of the public Coolprop thermodynamics library (http://coolprop.org/). All essential variables have been parametrized. The software has been expanded in several stages when there was a need to test new ideas and inspect possible technical problems. The most important algorithms are briefly described here. The HTML page of the program and the JavaScript source code it contains can be read directly from the server. The gases supported by the Coolprop library, their sources, and the allowed pressures and temperatures are listed in the List of Fluids section at http://www.coolprop.org/fluid_properties/PurePseudoPure.html . For example, the maximum allowed temperature of methane is 625 K, so the program sets the upper storage temperature to 625 Kelvin, if the methane is selected as the gas.

Simulation of compressor and turbine operation

The ideal gas equation cannot be used with real gases if the gas pressure is high or if the gas's condensation temperature is close. Therefore, when simulating the operation of compressors and turbines, thermodynamic libraries are used, which give very accurate results in all conditions. At its simplest, the simulation is done by calculating the four properties of the gas in the loop, when the efficiency of a stage η is known: pressure P (Pa), temperature T (K), mass specific enthalpy h (J/kg) and mass specific entropy s (J/kg/K). The system can be assumed to be closed because the mass flow and enthalpy change of the gas are very large compared to the heat leakage of the devices.

The program uses the easy-to-use high-level PropsSI method of the Coolprop library. With PropsSI two gas properties can be used to query the value of a third property. When η is the efficiency of one stage of a compressor or turbine, Δh is the positive or negative change in enthalpy, (T1, P1, h1, s1) is the initial state of the gas before the compressor or turbine stage and (T2, P2, h2, s2) is the end-state before the next stage. In a compressor, the efficiency is the part of the enthalpy change that adds the pressure while the entropy remains constant. The rest of the enthalpy change is converted directly into heat, which in turn increases the temperature and entropy of the gas in the final state. P2, h2, T2, s2 are calculated:

P2 = PropsSI ('P', 'H', h1+ Δh * η, 'S', s1, ' Nitrogen ')

h2 = h1 + Δh

T2 = PropsSI ('T', 'H', h2, 'P', P2, ' Nitrogen ')

s2 = PropsSI ('S' , 'H' , h2 , 'P' , P2 , 'Nitrogen')

In the case of a compressor, Δh is the work added into the system, which with the part determined by the efficiency increases the pressure. In the case of a turbine, Δh * η is the work produced by a turbin stage as a result of the pressure drop, while (1- η)* Δh is converted to heat.

There are several variations of that calculation because the change in enthalpy is not always known in advance. For example, the compressor must be simulated backwards with efficiency 1/η starting from its final pressure and temperature.

Calculation of the dimensions of the energy storage

The energy storage is assumed to be shaped like two opposite cones. That shape minimizes construction costs and heat loss. At the same time, it enables pressurizing the high-pressure reservoir with the mass of the lower pressure reservoir.

The main dimensioning parameters of the energy storage are the amount of mining in tons, the low pressure and pressure ratio in charge, the temperature of hot storage, the efficiencies of turbines and compressors, density of the rocks used for the upper and lower pressure storages, specific heat capacity, steepness of the wall, the sieve spacings of the gravel of the upper and lower pressure storage, the maximum steepness of the above-ground heap and the permitted heat leakage per square meter. It is assumed that all mined aggregate will be used to build energy storage.

At first the average volume specific heat capacity is calculated is for the temperature ranges of both storages. The specific heat capacity of aggregate depends on the temperature of the stone. Below on the left are the measured specific heat capacities of several rock minerals at different temperatures, and on the right their normalized distribution from the study A Review and Evaluation of Specific Heat Capacities of Rocks, Minerals, and Subsurface Fluids. Part 1: Minerals and Nonporous Rocks [31].

---

31 https://www.researchgate.net/publication/226113239_A_Review_and_Evaluation_of_Specific_Heat_Capacities_of_Rocks_Minerals_and_Subsurface_Fluids_Part_1_Minerals_and_Nonporous_Rocks

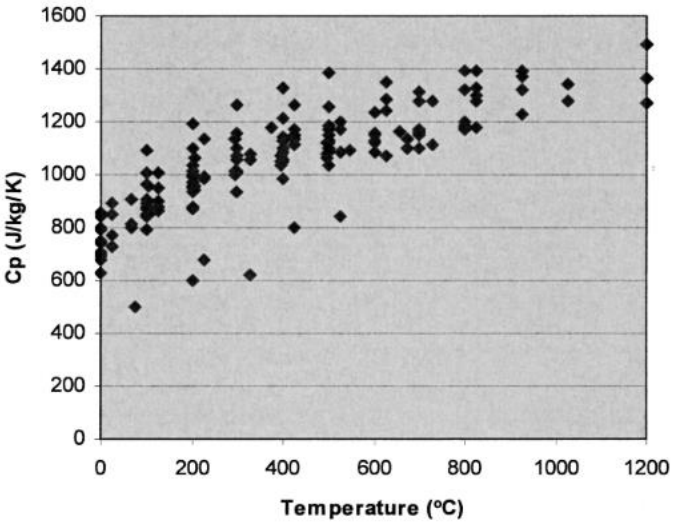

Figure 11. Measured specific heat capacities plotted as a function of temperature for all nonporous rock samples in Table 2, showing the general increase in heat capacity with increasing temperature. Data from Kappelmeyer and Haenel (1971), Tkach and Yurchak (1972), Roy, Beck, and Touloukian (1981), Čermák and Rybach (1982), and Robertson and Hemingway (1995).

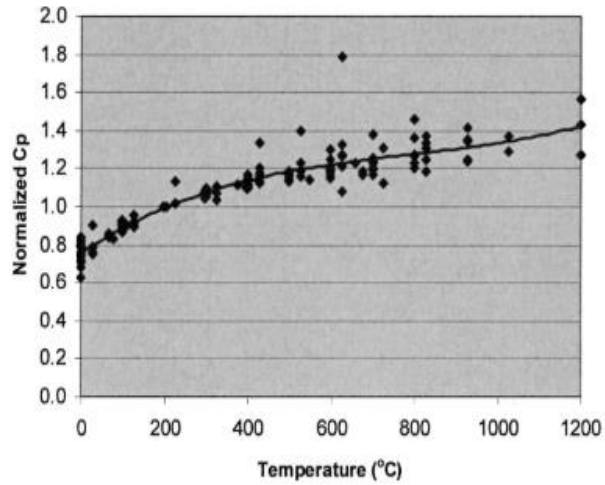

Figure 13. Normalized specific heat capacities plotted as a function of temperature for the same nonporous rocks shown in Figure 11. Normalization was carried out by dividing all reported specific heat capacities by the value for the same rock at 200°C. Line represents best-fit third-order polynomial. Correlation coefficient $r^2 = 0.93$.

Based on the research, the calculation of the specific heat capacity of the heat storage gravel is simplified so that above 550 °C it is assumed to be 1.3/0.8 times compared to the known specific heat capacity at 20 °C degrees, and below 550 °C it is assumed to decrease linearly, so that the line intersects the known specific heat capacity at 20 °C degrees and continues to decrease further linearly after this. The storage heat capacity is obtained by calculating the average specific heat capacity of the storage temperature range and multiplying it by the storage temperature change and mass.

Calculating the density of the gravel is based on the sieve spacing given as a parameter, and the assumption that if the rock density is 2650 kg/m^3 then the density of the compacted 0–100 mm crushed stone is 2100 kg/m^3, and the density of a compacted gravel with fully uniform particle size is 1500 kg/m^3 (with porosity 0.434). Based on this, the relative density (compared to its rock) of a well compacted gravel would be (1.5 + (2.1-1.5) * (1-(min particle size)/(max particle size)))/2.65, i.e. the minimum particle size leaves an empty space in the gravel, which reduces the density and specific weight. 1.5 might be a too high value for the density of a compacted gravel of uniform size, because the is assumed that the porosity of a completely uniform insulated gravel is 0.5, which would density 1325 kg/m^3. The density of a gravel, of course, depends on the actual sieve spacing, the average aspect ratio and size distribution of the particles, the settings of the crushers and the typical splitting of the aggregate. The actual values can only be determined by measuring. A gravel with a round particle shape and smaller aspect ratio has been found to pack more tightly, and its hydrological resistance is also lower. Rounder particles can probably stand higher point load too. Thus, with the right adjustments of the crusher and its sieves, the operation of the storage can be improved and probably also extend the service life. The gravel probably does not need to be compacted after application, because it compacts itself due to the weight of the large machines and the gravel mass coming on top.

Calculating the shape and dimensions of the storage is a typical multi-step heuristic algorithm. Its preferred result (the weight of upper storage per square meter) is known in advance, but all dimension variables needed to calculate it are unknown. The energy storage must meet the following requirements:

1. The heat capacities of the upper and lower pressure storages must be symmetrical, i.e. when the high-pressure storage is full of heat, the lower pressure storage is full of cold and of course vice versa.
2. The above-ground part of the storage should preferably be completely above the high-pressure storage.
3. The weight (in Newtons) per square meter of the upper low-pressure storage should be about the same as the maximum pressure of the high-pressure storage. The program assumes that the compacted gravel on the storage scale behaves like a liquid: only the mass directly above the high-pressure storage matters in the calculation. The actual compression force can be measured with the pressure sensors above the high-pressure storage.
4. The area of the storage's external surface should be as small as possible.

At first, an initial weight is calculated using an educated guess about the dimensions of the storage. The algorithm makes necessary corrections to the dimensions, and the calculation is made again. This is repeated until the safety margin of the result is less than 5% above or below 100 kPa.

Along with the storage dimensions, the program calculates the proportion of gas to be liquefied during the charge, which is 0.4% of the mass flow with the default parameters.

Dimensioning of pipelines

The allowable pressure drop caused by the pipes between the reservoirs and the turbo machines is one of the design parameters of the system. Its default value is 1%. Based on the given allowable pressure drop, the diameters of the pipes and the gas velocity in the pipe are calculated. The pressure changes caused by height differences are included in the calculation. The actual pressure drop is calculated using the Darcy-Weisbach equation (https://en.wikipedia.org/wiki/Darcy%E2%80%93Weisbach_equation). The friction factor f used in the equation is calculated as presented by Tkachenko and Mileikovskyi in 2020. The value of epsilon (ε) is 0.025 (steel, structural or forged), which is probably an order of magnitude worse than the typical value of steel pipes. On the other hand, pipe bends, welds, and valves each increase the pressure drop, so it probably gives a good estimation of the actual value. The algorithm is again heuristic because the desired end result is known, i.e. the allowed pressure drop, but the equation is too complex to directly solve the only variable affecting it, i.e. the diameter of the pipe.

Calculation of gas flow resistance in a gravel

Air flow in the gravel has apparently not been studied very much, because with the search words used, only a seminar presentation of a research project was found [32]. In it, the radon ventilation of the subfloor was studied with two EU standard gravels 6/12 and 10/20. The conclusion of the study was that for the gravel, the Darcy-Forchheimer equation best corresponds to the measurement results. The superiority of the equation is self-evident, because the laminar and turbulent parts of the equation have their own measurement-based coefficients depending on the properties of the gravel.

The Darcy-Forchheimer equation is : $\Delta P/L = \mu/k * v + c/k * v^2$, where ΔP is the pressure change (Pa), L is the distance (m), μ viscosity (Pa*s), measured k permeability of the gravel (m^2), v velocity (m/s) and c measured Forchheimer factor.

---

32 https://www.researchgate.net/publication/322140487_Behaviour_study_of_airflow_through_gravels_based_on_laboratory_experimentation_and_contrast_with_FEM_models

The study measured the permeability of the gravels , the Forchheimer factor and the pressure drop at air flow speeds of 0.015–0.5 m/s. The gas flow velocity range of the energy storage (0.02–0.15 m/s) is within those speeds, but the min and max particle size of the gravels and the porosity differ significantly from the EU standard gravels in the study. The gravels measured in the study were apparently more or less uncompacted because their porosity was 0.40 and 0.51. Therefore, in the calculation of the pressure drop in the storages, the values measured for the 20/40 gravel of the study are used as a fixed point, whose laminar (200) and turbulence coefficient (1630) are scaled for the selected gravel fraction and its porosity using Erguin's equation [33]:

$\Delta P/L=v*(150*\mu/D_p^2)*(1-n)^2/n^3+v^2*(1.75*\rho/D_p)*(1-n)/n^3$, where v is velocity (m/s), μ is viscosity (Pa*s), D_p is the average diameter of the particles in the gravel, n is the porosity of the gravel and ρ is the gas density.

In addition, the viscosity and density of the air of study are scaled to the selected working fluid at the pressure and temperature of the storage part.

The program calculates the pressure drops in the hot and cold parts of both storages. When calculating the electricity recovery efficiency, the storage is assumed to be half full.

Compressor and turbine blade stresses

The load on the blade consists of the centrifugal force caused by the rotation and the torque caused by the gas velocity change, compression, and the pressure difference between blade sides. The tensile stress caused by centrifugal force depends solely on the distribution blade's mass in longitudinal direction, so the maximum torque determines the blade's thickness. In the calculation of centrifugal force and torque, it is assumed that the cross-sectional area of rotor's tip is 15% of the cross-sectional area of its hub, and the thickness decreases linearly from the hub to the tip. The program assumes, that the pressure side surface of a blade needs to bear only the torque stress, and the opposite side takes care of the centrifugal stress. The maximum allowed torque is calculated from the maximum allowable stress of the selected blade material at the temperature and in used blade service cycle. Since the torque decreases linearly from the hub to the tip, the torque at the hub is obtained by calculating the torque produced by the thrust of the stage at the center of the gas flow. The thickness of the blade at the hub is set so that the tensile stress on the pressure side surface of the hub is the same as the maximum allowable stress of the material.

The centrifugal force on the rotating blade of the rotor is[34] $\sigma_{ct} = 0.5 * \rho_b * U_t^2 * K * (1-b^2)$, where ρ_b is the density of the material, U_t the rotational velocity of the rotor tip, b the ratio of the rotor hub and tip radii. The coefficient K is calculated using the equation $K=1-(1-d)*(2-b-b^2)/(3*(1-b))$, where d is the aforementioned ratio of the cross section of the tip of the blade to the cross section of the hub. The ratio d=0.15 used in the blade thickness calculation gives K as 0.55, which is at the lower limit of the typical range (0.55–0.65) of turbine and compressor blades reported by the source. Since the cross-section of the rotor blade is mostly a square, its section modulus is calculated using the equation for rectangle[35] $S = b * t^2/6$, where t is the thickness of the blade and b is the width. The section modulus therefore increases to the second power of the thickness. The maximum torque is $M_y = S * \sigma_y$, where σ_y is the maximum permissible tensile stress.

---

[33] https://en.wikipedia.org/wiki/Ergun_equation

[34] Module_04_-_Axial_Flow_Comp.pdf (polymtl.ca)

[35] https://en.wikipedia.org/wiki/Section_modulus

The force that twists the rotor blade is obtained by assuming that the work W done per second by the compressor stage would be completely converted into kinetic energy of the gas, so that the new velocity of the gas would be v2 = sqrt (2 * W/m + $v1^2$). From that we get the acceleration a=(v2-v1)/1 s, and from that, based on the gas mass flow, the force of all the blades in the stage is F=a*m. The force applied to one meter of the blade width is F / solidity*2*π*$r_{hub.}$. Solidity at hub is the sum of stage blades' width / 2*π*r_{hub}.

The maximum allowable stress depends on the selected material, temperature and maintenance interval. The default value of the maximum allowable stress of hot devices has been selected according to the Nimonic 105 [36]alloy and the 3000-hour maintenance interval. In the first low-pressure stages of cold turbo machines, nickel-containing high-strength steels such as maraging steel[37] can possibly be used, in which case their rotor blades could be made much thinner than the blades of hot devices. However, the problem with maraging steel is the rapid deterioration of fracture toughness as the temperature drops. However, some other common austenitic steels withstand very low temperatures, and the 0.2% proof tensile strength of thin hardened pieces (carbide solution treated and strain hardened) is at best over 600 MPa[38], and some special metal alloys have been developed for cryogenic temperatures[39]. Their strength and other properties improve as the temperature decreases. The maximum tensile strength of these special metal alloys is at best almost 1000 MPa, but their maximum continuous stress probably 350 MPa at most, which the program uses as the default value for the maximum allowed stress of cryogenic blades.

[36]https://www.specialmetals.com/documents/technical-bulletins/nimonic-alloy-105.pdf
[37]https://en.wikipedia.org/wiki/Maraging_steel
[38]
https://nickelinstitute.org/media/1723/materialsforcryogenicservice_engineeringpropertiesofausteniticstainlesssteel_4368_.pdf

Choosing nitrogen as the working fluid of the system

Air and other mixed gases are not suitable as working fluids for this solution, because they do not have an exact dew point. Each component of a mixed gas liquefies at its own temperature. Carbon dioxide is not suitable as a working fluid because its triple point pressure is more than five atmospheres, which would be far too high for the pressure of a low-pressure storage. Oxygen or air, on the other hand, would glow the biochar used as insulation into carbon dioxide.

In the energy storage planning and simulation program, you can choose argon, helium, methane, nitrogen, or hydrogen as the working fluid. Of these, nitrogen has by far the best electricity recovery efficiency of 88% and the second best storage capacity after helium. In addition, the properties of nitrogen and air are very similar, so it is easy to adapt the technology of today's large industrial compressors and turbines to nitrogen.

The recovery efficiency of helium is only 76.6%, because the cooling work required for it to reach the low pressure dew point is very large. In addition, as an expensive and rare gas, it is an impossible choice for working fluid anyway.

The recovery efficiency calculated for argon is 83.5%, and in addition to the lower efficiency and storage capacity, isolating it from the air requires many times more energy compared to nitrogen.

The upper temperature of methane is 625 K, because Coolprop does not support higher temperatures with methane (probably because of a good reason). Partly because of this, the methane recovery efficiency remains at 80.1% and the capacity at about half of the nitrogen capacity.

The hydrogen recovery efficiency is 82.6%, because the upper temperature of the hydrogen also has to be lowered to 700 Kelvin and at the same time the mass flow must be increased, so that Maraging 2400 high-strength steel can be used in the hot compressor and turbine. At the rotor rotational velocity required by hydrogen, the centrifugal force exceeds the tensile strength of alloy metals resistant to hot temperatures many times over, so the number of stages in the devices would have to be multiplied. In principle, by cooling the Maraging 2400 steel, the upper temperature could be raised to about 1000 Kelvins, but in this case the number of stages must be increased at the same time, so that the centrifugal force does not exceed the tensile strength of the Maraging 2400 high-strength steel. About 1050 K is probably the maximum temperature of hydrogen in any way, because the hydrogen reduction of iron ($Fe_2O_3 + 3\ H_2 \rightarrow 2\ Fe + 3\ H_2O$) takes place at a temperature of about 800 °C [40], and it takes about 54 kg of hydrogen gas to reduce one ton of hematite. The hot water vapor produced by the reduction reacts with the iron of pyroxene and olivine , forming new iron oxide and hydrogen. Thus, the selected aggregate also prevents the use of higher temperatures with hydrogen.

Siemens Energy has recently released a hydrogen compressor concept based on counter-rotation [41]. The efficiency of one stage is at best 89% (i.e. " polytropic efficiency "), and the pressure ratio of its counter-rotating half is 1.09 (with 24 counter-rotating pairs, a pressure of 80 atmospheres is achieved, i.e. a total of 48 stages in the concept and apparently as many separate motors). The concept is still just a plan, but it shows that hydrogen is a very challenging gas for compressor and turbine technology compared to air or nitrogen.

---

[40] https://lutpub.lut.fi/bitstream/handle/10024/163963/Kandidaatinty%C3%B6_Kurvi_Miika.pdf?sequence=1&isAllowed=y

[41] Advanced Hydrogen Compressor for Hydrogen Storage Integrated with a Powerplant https://www.osti.gov/servlets/purl/1874341

The third problem with hydrogen is the difficulty of isolating it. No metal alloy is suitable for isolating hydrogen in a very wide temperature range of the storage. Carbon-free soft iron insulates hydrogen well and also does not become brittle under the influence of hydrogen. Its problem is that iron becomes very brittle already at a few tens of degrees below zero.

Motor-generators of pumped hydro stations

The first pumping stations were built at the beginning of the 20th century. Since then, their power and efficiency have continuously improved with the development of technology. Nowadays, the largest pumped hydro stations usually consist of a reversible pump-turbine and a synchronous motor-generator. Voith Hydro is the largest supplier of pumped hydro stations, and its technical solutions and references are described in the brochure *Harnessing the power of water with engineered reliability* [42].

In terms of PTES, the most interesting are Voith's motor-generator solutions, whose outputs reach up to 530 MVA (Bath County, USA, rpm 257). Most of Voith's references have only one speed, i.e. their motor-generator is synchronous. Thus, their number of revolutions is always a fractional number of the network frequency, and the number of pole pairs of their motor generator varies between 5 and 14. Voith has also supplied asynchronous motor generators such as Europe's largest 433 MVA unit (Frades II, Portugal, rpm 350–381). Voith supplies asynchronous motor-generators based on induction [43]and synchronous motor-generator with frequency converters.

The main advantage of asynchronous motor-generators is the adjustable power range, they are also self-starting. Large Synchronous motors and motor generators always need either an external or an integrated starting system, or most often a combination of both [44]. Synchronous generators of large thermal power plants have usually large number of single pole pairs. The turbine and possible compressor unit are directly connected to the generator shaft, i.e. their rotation speed is determined by the network frequency. The efficiency of large synchronous generators is at best 99%. Power adjustment is done by changing the pressure ratio and mass flow of the turbine. However, the adjustment usually takes place at the expense of efficiency. Only small power plants must use a gearbox between the generator and the turbine, because otherwise the rotation of the generator is too low for a small turbine.

The world's largest induction motor made by GE in 2018 has a power of 80 MW and an efficiency up to 98.1% [45]. Either this is not completely true, or the big asynchronous motor-generators supplied by Voith are controlled with static frequency converters. The typical power range of frequency converters extends up to 10 MW, so for example the asynchronous 433 MVA unit of Frades II would be too big or them. However, in 2018, ABB has delivered a 4*103 MW static frequency converter system to the German railways, which had 4 different frequencies [46].

Voith's brochure does not state the efficiencies of its references, but the power of their pump turbines is at most 90% of the power of motor generators. It may mean that the pumping is carried out at almost full power, with the unloading power being approximately the power of the turbine, i.e. at most 90%. Voith motor

---

[42]https://voith.com/corp-en/11_06_Broschuere-Pumped-storage_einzeln.pdf
[43] https://en.wikipedia.org/wiki/Induction_motor
[44] https://en.wikipedia.org/wiki/Synchronous_motor
[45] https://www.gevernova.com/power-conversion/news/ge-successfully-completed-no-load-testing-one-worlds-largest-80-megawatt-induction
[46] https://new.abb.com/news/detail/10379/worlds-most-powerful-rail-frequency-converter

generators can be cooled with air or water. Air cooling can be used in the generators of hydropower plants even at high power, if their rotation number is low enough. Large thermal power generators of more than 60 MW directly connected to the grid frequency must use hydrogen cooling or a combination of hydrogen and water cooling [47]. The engine generators of the hydropower pumped power plants cannot be used as such in heat-based gas pumped power plants, but their technical solutions can be directly applied there.

Turbine and compressor technology of current gas turbine power plants

According to Wikipedia, the single-stage efficiency of axial compressors[48] is 0.92 at best, and the typical pressure ratio of industrial compressors is 1.05–1.2. However, this is outdated information. The supersonic compressors of the new large gas turbines reach a mass flow of 700–1000 kg/s and 24–25 times the pressure in only 13–15 stages [49]. A Chinese research group was able to improve the efficiency of the low-pressure stage of an old gas turbine model compressor from 94% to 95% using CFD modeling, and at the same time achieve[50] a pressure ratio of 1.5. The F-model mentioned in the study was probably Mitsubishi F model.

The compressor power of new gas turbines is at best less than 45% of the gross power of the turbine, and the gross power of the turbine unit is typically approximately twice the net power of the plant. In this case, for example, the compressor power of the 448 MW Mitsubishi M701JAC gas turbine could be around 400 MW, and the power of its turbine device around 900 MW. The list price of the M701JAC plant package without the heat recovery unit is estimated at 76 million dollars[51]. If we assume the cost of energy storage compressor and turbine units to be 60% of the total price of a simple gas turbine package, then the price of the compressor and turbine power would be 35 $/kWh. Program uses that as the default cost of axial turbomachine power.

The combustion chamber and power transmission of a gas turbine power plant set technical limitations for the design of its compressor and turbine, which are not a limitation when designing a separate high-power compressor or a turbine operating mainly without cooling. The compressor and turbine of large gas turbine power plants are directly connected to the shaft of the bipolar generator, so their rotational velocity is the same as the frequency of the electrical grid, i.e. either 3000 or 3600 revolutions per minute. To keep the power of each stage constant, the hub to tip ratio of compressor blade increases in each stage. The hub/tip ratio of the last high-pressure stages is usually very high. For example, with the M701JAC compressor, it would appear to be 0.93 based on the picture, which means that the gas then flows through a very thin ring. That means, that the efficiency of the last stages is several percent worse than the aforementioned optimum due to high end-wall and tip clearance losses. Solving the efficiency problem of high-pressure stages is therefore crucial for the implementation of energy storage, and therefore we will present above how this can be solved within the framework of current technology and material technology.

Thanks to the complex air cooling technology of gas power turbines, it has been possible to raise the temperature of the turbine's combustion gases to almost 1700 °C, but at the same time cooling to almost 1000 °C and producing the cooling air required for it significantly reduces the overall efficiency of the gas turbine. The efficiency of the turbine is also reduced by the small number of stages (maximum 4), when the loading

---

[47] https://en.wikipedia.org/wiki/Hydrogen-cooled_turbo_generator
[48] https://en.wikipedia.org/wiki/Axial_compressor
[49] Mitsubishi J-Type Technology https://www.mhi.co.jp/technology/review/pdf/e503/e503001.pdf
[50] Optimization Design of Aspect Ratio and Solidity of a Heavy-Duty Gas Turbine Transonic Compressor Rotor https://www.mdpi.com/2075-1702/11/1/82

[51] https://tealgroup.com/images/TGCTOC/sample-wpsbim.pdf

coefficients of the individual stages and the torques of the blades inevitably become large. A high torque increases the thickness of the blades and thus increases profile losses. For these reasons, the efficiency of the turbine equipment of commercial gas turbines falls significantly below the suggested optimal value of 0.97. The manufacturers only state the overall efficiency of the gas turbine power plant, based on which the efficiency of the plant's compressor or turbine unit cannot be deduced.

The tensile strength of the high temperature alloys used in the rotor blades of turbines and compressors usually begins to decrease rapidly above 650 °C and has almost disappeared by 1000 °C at the latest [52]. Newer directionally solidified alloys have a high tensile strength up to 800 °C. When the tensile stress of the operating temperature is exceeded, the rotor blades must be cooled. The internal cooling of the rotor can be used if the temperature difference is at most 100 °C and external cooling is used above it. External cooling has a thin layer of colder gas is directed onto the surface of the rotor. The nitrogen gas of the high-pressure storage at about minus 50 °C can be used for the cooling of the last high-pressure stages. Less than one percent of the mass flow would be needed for the cooling.

[52] https://nickelinstitute.org/media/8d934861431 8 2f5/nickel_incopub393_updated-june-2021.pdf

Performance limits of axial compressor and turbine stages

Compressor and turbine losses can be divided into four parts: gas friction on the surface of the rotor and stator blades, i.e. profile losses, friction caused by the outer and inner edges, rotor tip leakage and mixing of the gas flow above and below the blade. Research Performance Limits of Axial Turbomachine According to Stages [53], the maximum efficiency of the upstream stage of a large gas turbine compressor is 95.5%. In this case, its losses are distributed according to the figure on the left below. Accordingly, according to the study, the maximum efficiency of the uncooled optimized turbine stage would be 97.2%. The distribution of its losses is in the figure on the right.

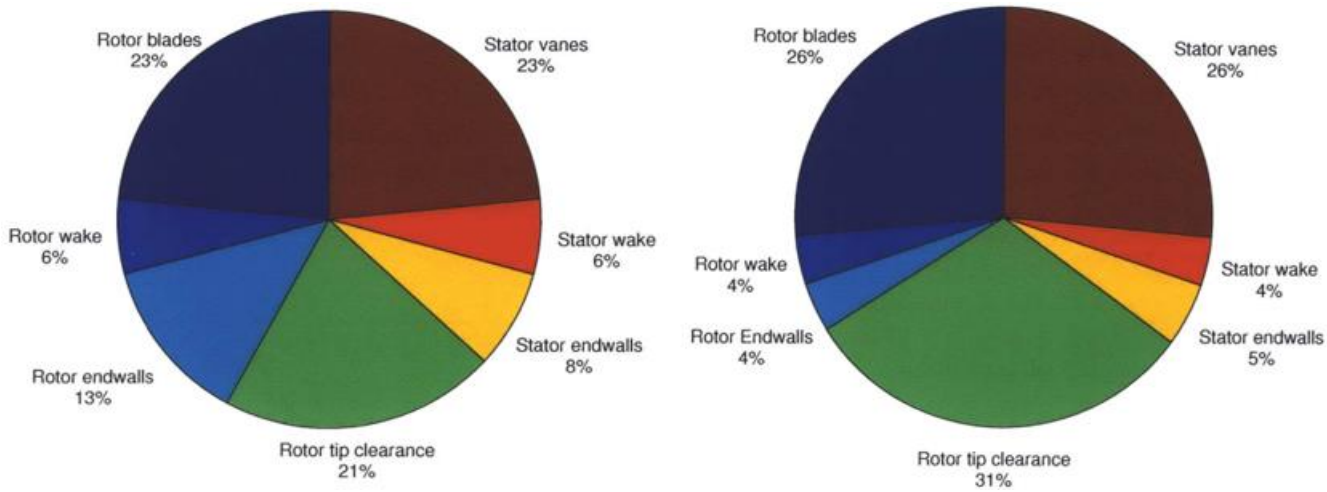

Figure 4. On the left, the losses of the optimized low-pressure stage of the compressor and the turbine on the right, according to the study "Performance Limits of Axial Turbomachine Stages"

The compressor tip clearance is assumed to be 1% of the blade length a typical for the front stages. According to the model in question, every percentage increase in the relative tip clearance decreases the stage efficiency by a percentage. In other studies and measurements of physical devices, the decrease in efficiency has been found to be up to 2%. The large tip clearance percentage typical of high-pressure rear stages is the main reason why their efficiency is several percent worse than upstream stages.

In the pictures *Rotor blades* and *Stator vanes* are the profile losses of the fluid flowing along the blades. The profile losses increase in proportion to the thickness of the blade and in inverse proportion to the Reynolds number when it falls below $5*10^5$, because then the laminar flow surfaces and the resulting losses start to increase rapidly. One of the goals of aerodynamic design is to keep the flow completely turbulent. A turbulent flow literally detaches from the surrounding surfaces. The Reynolds number for compressors and turbines is usually calculated by multiplying the chord of the rotor blade by the relative velocity of the gas at the front tip of the blade and dividing by the kinematic viscosity (viscosity/density). Profile losses no longer significantly decrease when the Reynolds number exceeds 10^6.

[53]Performance Limits of Axial Axial turbomachine Stages https://core.ac.uk/download/pdf/4427598.pdf

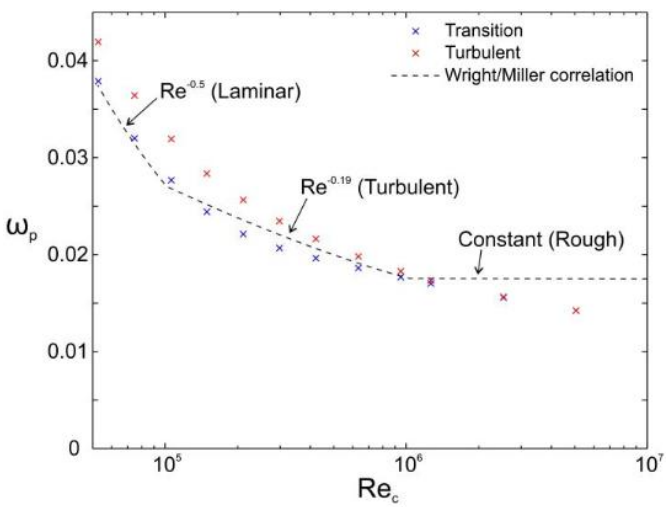

Fig. 18: Profile loss variation with Re_c (MISES)

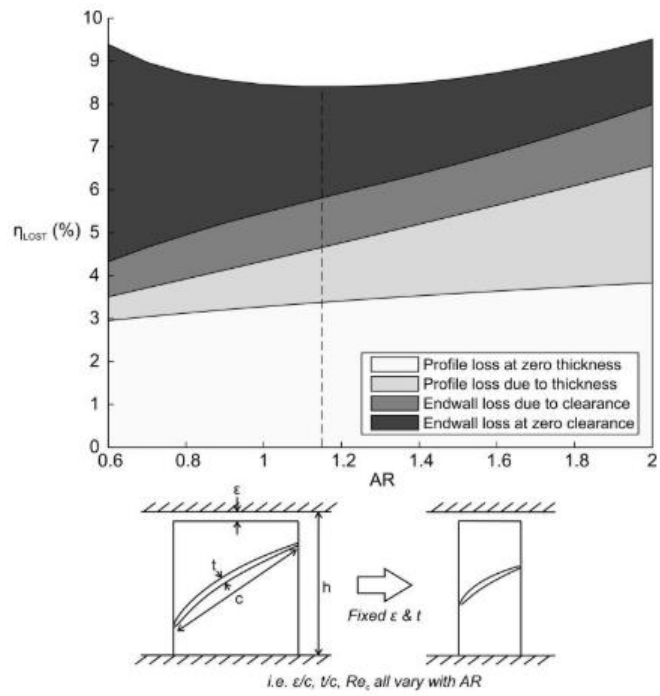

Fig. 21: Breakdown of lost efficiency using low order model (t/h = 4.7%, ε/h = 1.2%, Re_h = 5.5x10^5)

The figure above shows the ratio of profile losses to Reynolds number according to the study THE EFFECT OF ASPECT RATIO ON COMPRESSOR PERFORMANCE [54]. On the right side of it is another picture copied from the same study, which shows the dependence of the aspect ratio of the blade (height h/width c) on profile and endwall losses. The figure shows the share of 1.2% tip clearance and 4.7% rotor thickness in the total losses with different aspect ratios, when Re_h is constant $5.5*10^{5.}$ The Reynolds number Re_h in the image has been calculated according to the height of the blade, so that in the CFD simulation it would be constant when the aspect ratio and the width of the blade change. In the figure, the profile losses increase and the endwall losses decrease when going to the right. At the same time, the Reynolds number Re_c calculated according to the blade width decreases from $9.2*10^5$ to $2.25*10^{5.}$ In the picture, the optimal blade aspect ratio AR=1.15 can be found in the middle, where Re_c is $4.3*10^5$, i.e. then the laminar flow surfaces have started to increase profile losses.

Along with the tip leakage, the endwall losses of the compressor are caused by the slow flow area on the inner and outer edges [55], which narrows the free flow area on both sides. Based on the image on the right, endwall losses independent of tip leakage increase linearly in relation to the width of the blade. Especially at the inner edge, the area widens and the endwall losses increase in the last high-pressure stages of the compressor. The importance of the losses at the inner edge is emphasized especially when all stages of the compressor operate at the same rotational velocity, in which case the blades of the later stages shorten towards their horizontal centerline. In this case, the ratio of the rotor's hub and tip usually increases to 0.9 or more in the last stage.

[54] https://api.repository.cam.ac.uk/server/api/core/bitstreams/fbfb70fe-58b3-47fb-a338-859384279d7c/content
[55] http://www.turbo.dae.tsinghua.edu.cn/upload/59d9ee5af3f4e.pdf

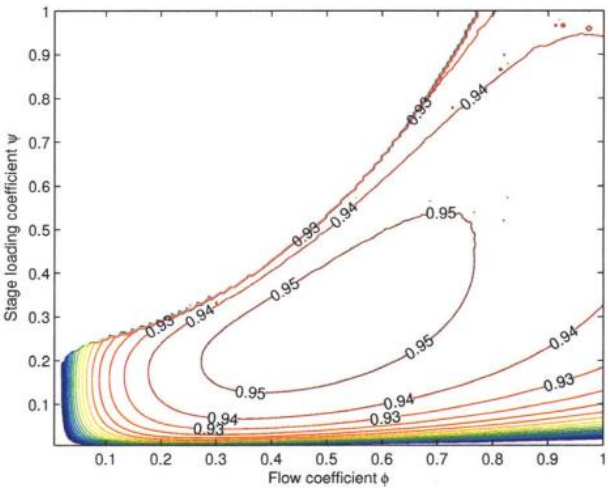

Figure 4-2: Smith chart, optimized baseline compressor stage

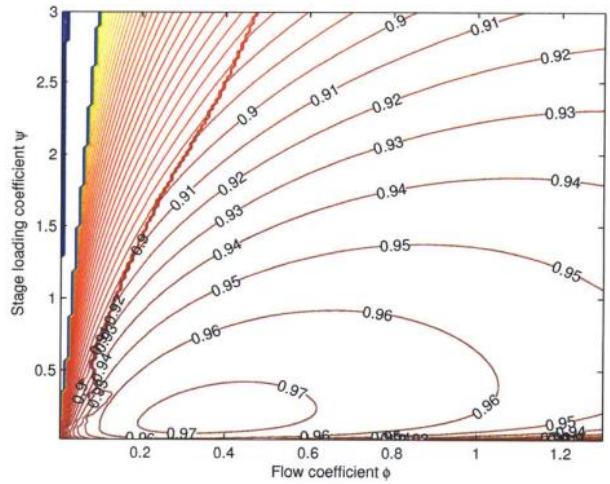

Figure 5-2: Smith chart, optimized baseline uncooled stage

When the compressor or turbine losses are optimized as low as possible, the efficiency of a front stage can be calculated from its stage loading and flow coefficients. Stage loading coefficient is $\psi=\Delta h/U^2$, where Δh is the fluid enthalpy change in J/kg and U is the rotational velocity of the rotor tip in m/s. The flow coefficient is $\phi=V_x/U$, where V_x is the velocity of the gas in its actual direction of travel, i.e. axial velocity.

In the picture above, on the left is the Smith diagram of an optimized compressor baseline stage and on the right of the uncooled baseline turbine stage, i.e. the dependence of the efficiency of the stage on the flow and load coefficients of the study Performance Limits of Axial Turbomachine Stages according to loss model and optimization algorithm. The efficiencies have been calculated assuming that the tip clearance is 1% of the stage length. Other parameters can be found in the mentioned study.

Main components of pumped thermal energy storage

In the center of the power unit is a large bipolar generator-motor, which functions as a motor during the charging mode and as a generator during the discharge mode. On the other side of the generator is the main hot gas turbine and its counterpart, the cryogenic compressor. The pipe shafts of the main turbine are connected to the main shaft of the generator with a customized vacuum gearbox. Its counterpart, the cryogenic compressor, is on the side of the main shaft. The cryogenic compressor has its own customized vacuum gearbox, where there are extra gears with a diameter of at least one and a half meters between the main shaft and the pipe shaft gear box, because otherwise the cryogenic compressor would not fit on the side of the main generator shaft. For the sake of clarity, the extra gear in between is not drawn in the picture of the cryogenic compressor. For the same reason, the incoming pipe to the cryogenic compressor should first turn up above the main shaft before it can widen to the final width. On the opposite side of the generator is the main compressor and its counterpart is a cryogenic turbine connected to the side of the main shaft of the generator.

Axial turbines and compressors operate in a pressure well. The fluid velocity is increased to the optimal design velocity. The gas is accelerated by converting a small part of its enthalpy into kinetic energy by lowering its pressure and temperature. At the exit, the gas flow is correspondingly slowed down to the final transport velocity by widening the pipe, and its kinetic energy is converted back into enthalpy as increased pressure and heat[56]. Presumably, the gas velocity change in an aerodynamically designed space does not significantly change its entropy, i.e. the losses are very small compared to the losses inside a compressor or turbine. Losses caused by changes in fluid velocity were also not mentioned in the above-referenced sources, so the program assumes, that those losses are nil.

The compressor can be started by the turbine on the opposite side of the generator, so that their high-pressure is gradually raised to the level of the high-pressure storage. When the generator shaft rotation reaches the network frequency, the generator magnets are switched on. The electric power starts twisting the main shaft and the turbine can be disconnected and shut down. The compressor can possibly also be started directly by kick starting the generator-motor with plant's frequency converters.

The inlet fluid to all turbines and compressors must be filtered from dust particles suspended in the fluid just like in gas turbine power plants. One technical challenge is caused by the hot gas from the high-pressure storage entering the main turbine, whose temperature probably exceeds the operating temperature of all conventional filter materials. In this case, high-temperature-resistant ceramic or silicate fibers or combinations of their fibers and insulators can be used as filter material.

The large hot gas pipes of the low-pressure storage can be made of ordinary steel, but all other piping between the storage and the equipment must be made of austenitic steel. The tensile strength of austenitic steel is not necessarily sufficient as such at the upper temperature of the storage, in which case the hot gas pipes would have to be insulated from the inside and possibly also cooled.

The heat pump that pre-cools the gas going to the cryogenic turbine has its own asynchronous motor controlled by a frequency converter, because its power requirement varies according to the temperature of the cooling water and the cooling requirement of the main circuit. The heat pump unit consists of two single-stage compressors, between which there is an additional cooler using water, two-stage turbines and three heat exchangers. With optimal efficiency, the heat pump's own power is about 3% and the cooling power is 4–5% of

[56] https://en.wikipedia.org/wiki/Bernoulli%27s_principle#Compressible_flow_in_thermodynamics

the total power of the plant. The output of plate heat exchangers based on the reverse flow of heat pumps is about 25% of the plant's net output. For a 1000 MW plant, it would mean that with 2 mm plate gaps, a temperature difference of 2 Kelvin and a heat exchange coefficient of 100 W/m2, the total volume of the heat exchanger would be 2500 cubic meters and its weight in tons would probably be of the same order of magnitude. The list price of such cooling equipment is around 10 million euros [57]. The gas of the main circuit can be used as the working fluid of the cooling heat pump, and the average of its lower and high-pressure could be approximately the same as the high-pressure of the main circuit, so that the pressure differences and wall thicknesses of the heat exchanger would be as small as possible.

If there is no need for district heating, different pressure ratios are used in unloading and charging mode so that the lower temperatures and enthalpies of the main turbine and compressor are the same. The pressure difference requires that the excess gas in the charging mode is liquefied in a separate pressure equalization tank, so that it does not boil back into gas at a lower pressure. Separation of the liquid could take place by directing the approximately 4‰ wet gas coming out of the cryogenic turbine at a sufficiently slow velocity, for example, through a condensing fiber layer. At the same time, all oxygen and other gases that the nitrogen separation equipment has not been able to separate from the air or that have been released from the aggregate are also liquefied. The transition from charging mode to unloading mode takes place by running the cryogenic compressor for a maximum of a few hours after stopping the main compressor, until the desired pressure difference in the main turbine is reached. The driving time depends on the filling level of the electricity storage. It takes seven times longer to move a full storage to the unloading area than an empty storage. The transition from the unloading mode back to the charging mode takes place accordingly with a cryogenic turbine. The pressure difference can also be used to adjust the power of the main turbine and compressor to match the amount of electricity sold or purchased.

Compressor and turbine technology optimized for electrical energy storge

Here is an initial plan of a simple, compact, and very efficient compressor operating below the speed of sound as a basis for CFD modeling and design. The plant's turbines can be implemented on the same principle. A turbine is a mirror image of a compressor, at least in terms of its structural design, dimensions, material technology and strength calculation, but the direction of the mass flow is opposite. The design parameters of the compressor are set in such a way that the rotating blade in each stage of the compressor is operating with the best possible efficiency, but still within the framework set by material technology.

[57] https://www.ato.com/heat-exchanger-price-list

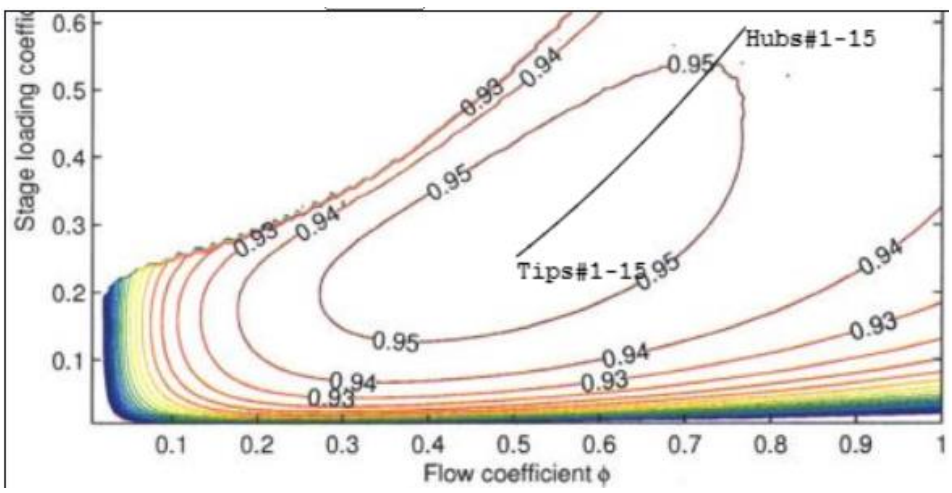

Figure 5. The arrangement of the stage efficiencies of the hot compressor in the Smith diagram.

The very high efficiency is made possible by stage specific rpm transmitted with nested pipe shafts to each compressor stage from a high-efficiency vacuum gearbox [58]. A separate gearbox enables free scaling of the size and power of each stage of the compressor. Figure 7 on next page has been drawn by the simulation program. It shows a 15-stage 294 MW main compressor with a mass flow of 372 kg/s and a pressure ratio of 1:26. Its power is divided equally between the stages to maintain the same optimal 0.65 hub-to-tip ratio for all stages. Also, the added tension caused by the centrifugal force and torque of the rotor blade is kept the same in all stages by increasing the thickness of the blade towards the end.

Other design parameters set in the simulation program are:

- Loading coefficient for the tip of the rotor: 0.25. The loading coefficient is the mass specific enthalpy change divided by the second power of the rotational velocity, i.e. $\Psi = \Delta h/U^2$
- Flow coefficient of the blade tip: 0.50. The flow coefficient is the velocity along the central axis of the gas divided by the rotational velocity, i.e. $\Phi = V_x/U$
- The default value of the efficiency of the compressor stage is assumed to be 0.955, i.e. only 4.5% of the input power would be lost as heat.
- The default aspect ratio of the blades of a stage, i.e. the ratio of the blade height to its chord h/c, is adaptive. The actual values are calculated according to the relative thickness of the blade (t/h) in the center of the gas flow. The aspect ratio drops from 2.23 in the first stage to 1.89 in the last stage. The scale to be chosen depends on the Reynolds number, whose large value enables a larger aspect ratio, which in turn enables smaller end-wall losses.
- The solidity at the hub of the rotor is 2. The solidity is the ratio of the chord of the rotor to the distance between the blades, i.e. c/s. If the blade shape is rectangle, the solidity at the tip of the blade is 0.65*2, which is in accordance with the recommendation, enabling a quite wide pressure range (surge margin) before the operation becomes unstable.
- Nimonic 105 nickel alloy used in the 60s and 70s. Its elastic elongation at that tension during 3000 hours at a temperature of 923 Kelvin is a maximum of 2 ‰. The newer alloys used today have higher

[58] RENK HET GEAR https://www.renk.com/en/products/turbo-high-speed/vacuum-gearbox-systems/het

operating temperatures, longer maintenance intervals and shorter and simpler rejuvenation heat treatments.

- The default value for the number of identical device units is 4. A smaller number of units just scales the dimensions and most other properties, but the relative dimensionless values remain the same. At the same time, the efficiency improves because the proportion of the free flow area of the gas increases. On the other hand, it is more difficult to adapt the power of a larger device to the electricity market.

The result is of course only indicative. Its main purpose is to demonstrate that a compressor and turbine with maximum efficiency are technically feasible within the limits set by material technology. The final design parameters must be optimized by CFD simulation when the materials of the blades and stators have been designed.

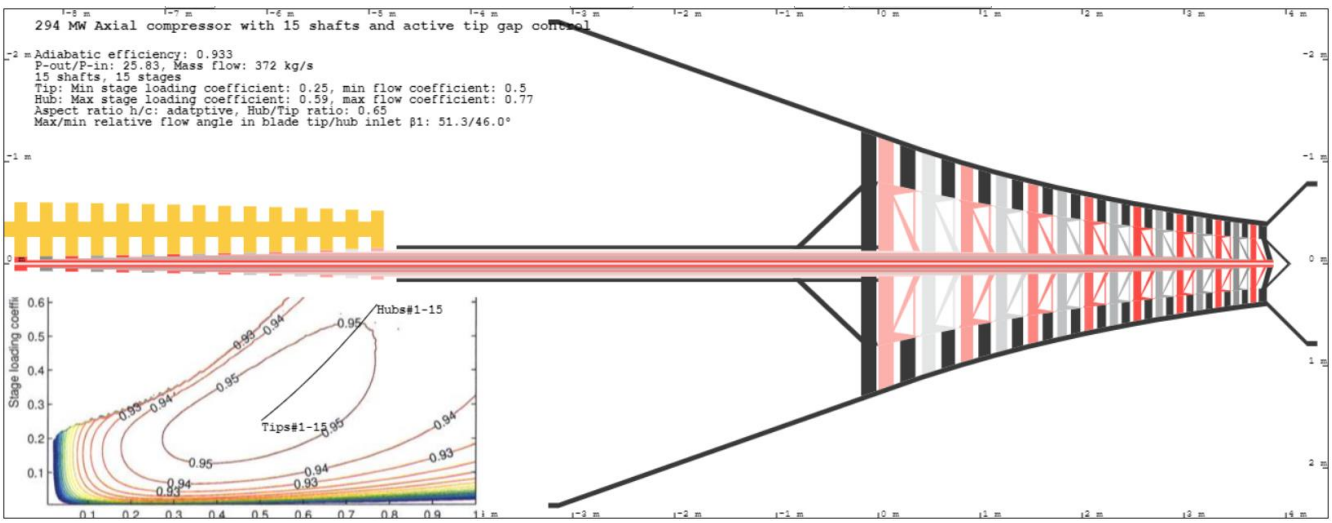

Figure 6. Dimensions of 294 MW hot compressor with 15-shafts and stages

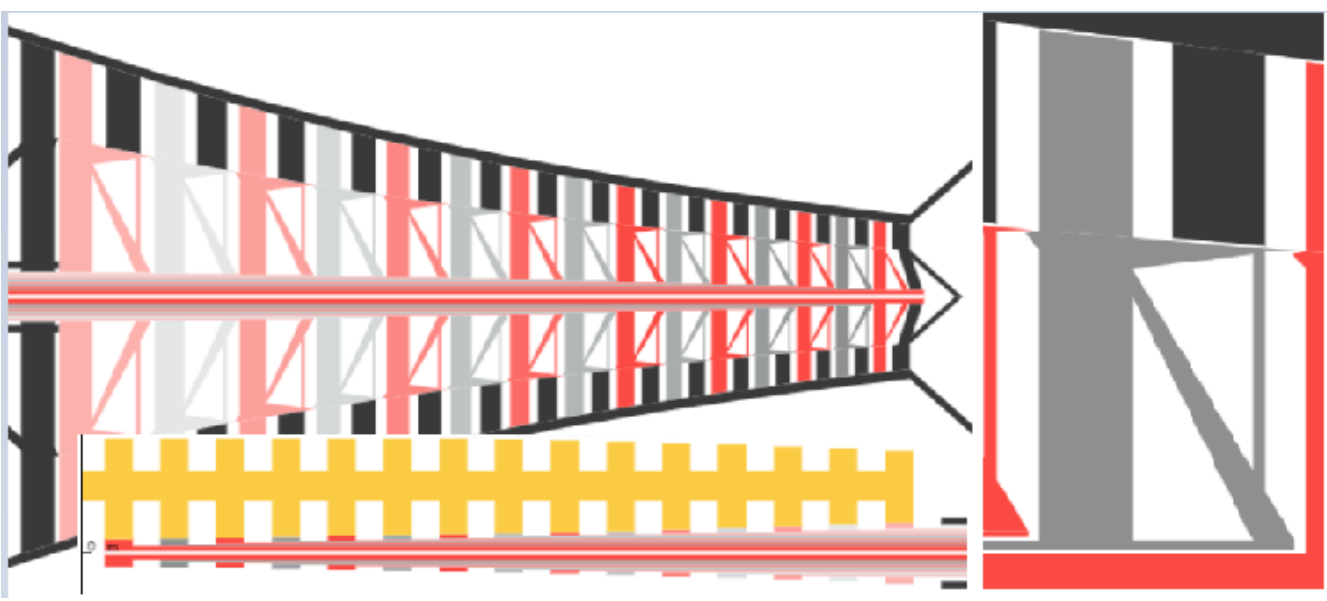

Figure 7. Enlarged view of the hot compressor and its gearbox and stage 14. The red and gray ones rotate, the case is black.

The upper picture shows the operating principle of the main compressor drawn by the program. In the pictures, the compressor case and the stators attached to it are black. The rotors and their base rotate at the speed of the pipe shafts are in the picture alternately in red and gray. In the lower picture, on the left, there is an enlarged cross-section of the compressor unit, on the right, a 1 pixel==1 mm enlargement of its penultimate stages, and below, the calculated transmission ratios of the vacuum gearbox from the main shaft of the motor-generator rotating 3000 times per minute. The maximum speed of the gears is less than half of the maximum allowed speed of 180 m/s of the vacuum gearbox. Also, the maximum rotational velocities of tube shaft bearings are about half of the 120 m/s maximum velocity of bearings mentioned in the literature. The maximum torque of the pipe shafts is about 85% of the maximum continuous tensile stress of 300 MPa, which in turn is 30% of the given maximum stress of 1000 MPa for a high-strength steel. The rotational velocities of the gearbox and bearings would allow the thicknesses and diameters of the shafts to be increased and even the replacement of the outer tube shafts with ordinary steel tubes. The cooling of the tube shafts and the rotating inner body of the stages can be implemented by letting the cold high-pressure storage gas from the high-pressure storage through the inner tube, from where it is discharged in a controlled manner through the cooling holes to the stage body and finally to the rotor blades. The stators and compressor case can be cooled from the outside.

Each pipe shaft is locked in place in the longitudinal direction by a horizontal steel bar with bearings next to the gears, which in the picture would be placed in front of the gears. The bearings of the horizontal supports receive the thrust load caused by the pressure difference between the blades and the stages, which is between 124 and 131 kN on the axes of the stages. The load is of the same order of magnitude as the weight on the bearings of one wheel of a fully loaded truck. Both ends of the horizontal supports are embedded in slanted grooves in the curved body of the gearbox. The position of the shaft and rotors can be adjusted on the x-axis by hydraulically pushing the horizontal support up or down in the arc-shaped groove. The contact surface between the tube shaft and its own gears can be grooved and sliding in the direction of the shaft, so that it remains in place relative to the generator gears as the shaft slides longitudinally inside it when the tube shaft gears are locked with the generator shaft gears. With 4 units, the gears of the gearboxes produce a maximum of 2.3 MW of radiant heat, which the long body of the vacuum gearbox should be able to cool easily.

The hydraulics are controlled by optical distance sensor, which with triangulation can remotely measure the distance between the tips of each stage and the case at the measurement point with an accuracy of micrometers using optical fibers embedded in the body. In addition, there should be pressure meters in the body in order to detect in time the occurrence of unstable operating conditions that shake the rotor heads. In addition, the ends of the rotors and stators, as well as the surface of the body against them, should be wearable in contact and replaceable. In this case, the small irregularities on both sides wear to the same level. Active tip clearance control enables the tip clearance of the rotors and stator blades to be adjusted in stable operating mode to a fraction of a millimeter, whereby the tip clearance leakage disappears almost completely. This may increase stage efficiency by 1–5%. The greatest benefit is achieved in the last high-pressure stages, where the proportion of losses caused by tip clearance leakage may rise to more than 50%. Active tip clearance control [59]is used in aircraft jet turbines, but nowhere to the extent or precision suggested here. In addition, operation below the speed of sound and a low loading coefficient reduce the vibration of the blades, thus enabling a smaller tip clearance. The amplitude of the blade vibration is inversely proportional to their stiffness. The contact angle between the rotor tips and the case is slightly steeper than the angle between the stators and the stage base, so there are inevitably small differences in their tip clearances. In driving mode,

[59] https://en.wikipedia.org/wiki/Active_tip-clearance_control

however, they can be optimized to the same distance by wearing the tips of both symmetrically, i.e. by burning off the first contact surfaces on purpose or by grinding the protruding tips during downtime. This requires that the rotating inner frames of each stage have a distance meter that can be read remotely, or that the tip of each stator has a protruding wear piece to be checked during maintenance. Its height indicates the minimum stator tip distance.

Hot compressor	Pipe in	Stage 1	Stage 2	Stage 3	Stage 4	Stage 5	Stage 6	Stage 7	Stage 8	Stage 9	Stage 10	Stage 11	Stage 12	Stage 13	Stage 14	Stage 15	Pipe out
Temp K	474	449	499	548	598	646	694	742	789	836	882	928	973	1018	1063	1107	1173
P kPa	98	81	116	160	215	282	364	460	574	707	861	1038	1240	1469	1727	2018	2526
Vx m/s	31	229	229	229	229	229	229	229	229	229	229	229	229	229	229	229	29
D mm	4680	2479	2178	1938	1741	1578	1441	1323	1221	1132	1054	984	923	867	817	772	1514
h kJ/kg	493	466	519	572	624	677	730	782	835	888	940	993	1046	1098	1151	1204	1283
P2/P1	0.83	1.43	1.38	1.34	1.31	1.29	1.27	1.25	1.23	1.22	1.21	1.19	1.18	1.18	1.17	1.16	1.08
Flow m3/s		614	477	379	307	253	211	178	152	131	114	99	87	77	68	61	
Power MW		19.6	19.6	19.6	19.6	19.6	19.6	19.6	19.6	19.6	19.6	19.6	19.6	19.6	19.6	19.9	
rpm		3542	4032	4533	5045	5567	6101	6646	7202	7770	8349	8940	9542	10155	10778	11412	
rTip mm		1237	1087	967	869	787	718	659	608	564	525	490	459	432	407	384	
Hub/Tip		0.65	0.65	0.65	0.65	0.65	0.65	0.65	0.65	0.65	0.65	0.65	0.65	0.65	0.65	0.65	
Blade h mm		433	380	338	304	276	251	231	213	197	184	172	161	151	142	134	
Chord mm		189	167	150	135	124	113	105	97	91	85	80	76	72	68	65	
Aspect ratio		2.29	2.27	2.26	2.25	2.23	2.22	2.20	2.18	2.17	2.15	2.14	2.12	2.10	2.08	2.07	
Mid flow t/h %		0.7	0.8	0.9	1.0	1.1	1.2	1.4	1.5	1.6	1.7	1.8	2.0	2.1	2.2	2.3	
Hub t/h %		1.4	1.5	1.7	1.9	2.1	2.3	2.5	2.8	3.0	3.2	3.4	3.7	3.9	4.1	4.4	
vRel tip inlet		0.85	0.81	0.77	0.74	0.71	0.69	0.67	0.65	0.63	0.62	0.60	0.59	0.57	0.56	0.55	
Re(c) EXP06		1.09	1.15	1.21	1.28	1.34	1.40	1.47	1.54	1.61	1.68	1.75	1.82	1.90	1.97	2.05	
Shaft radius mm		124	118	112	106	100	94	88	82	76	70	64	58	51	44	35	
Shaft torque %		48	47	46	47	48	49	52	56	60	67	75	83	83	83	82	
Shaft cent. stress %		3	4	4	5	5	5	5	6	6	5	5	5	4	3		
uShaft m/s		45.9	49.7	53.0	55.8	58.1	59.8	61.0	61.6	61.5	60.9	59.6	57.6	54.7	49.9	41.8	
uGear m/s		57.2	60.6	63.6	66.2	68.7	70.8	72.8	74.6	76.2	77.7	79.1	80.4	81.6	82.6	83.7	
Blades' load kN		63	63	63	63	63	63	63	63	63	63	63	63	63	63	63	
Shaft load kN		132	130	129	128	127	126	126	125	125	124	124	124	124	124	126	
Max blade stress MPa		456	456	456	456	456	456	456	456	456	456	456	456	456	456	456	
Centrifugal stress MPa		267	267	267	267	267	267	267	267	267	267	267	267	267	267	267	
Blade cooling K		0	0	0	0	0	0	0	0	0	0	28	73	118	162	206	

The program calculates the blade t/h of each stage, i.e. the ratio of the blade thickness to its height, in the middle flow and in the rotor hub. The calculated middle flow t/h ratios are very small in the low-pressure stages and reasonably small in the last high-pressure stages in terms of profile losses. In the calculation of the bending moment, the actual cross-section shape of the blade is not taken into account, but the bending moment is calculated according to the average thickness. The used maximum thickness t has been obtained from the average thickness by dividing it by the number 0.75, which was chosen visually based on the shape of the blades used in this speed range. The blade's bending stress is the same as the given maximum stress of 456 MPa. The greatest stress is on the outer surface of the pressure side at the hub of the rotor. On the opposite side, the bending is pressing the blade, so the blade gradually bends from the hub in the direction of low pressure. In the example, the maximum tension has been chosen so that the elastic, i.e. reversible,

elongation is 0.2%/3000 h. The gradual increase of the tip clearance caused by bending can be corrected with active tip clearance control. Thickening the middle part of the board increases its bending stiffness, because the bending stiffness is directly proportional to the square of the thickness. Centrifugal force does not depend on the absolute thickness of the blade, but, along with the rotational speed and radius, on the density of the material and the distribution of its mass between the hub and the tip. Centrifugal force has been calculated assuming that the blade tip cross-section is 15% of the hub cross-section and that the blade thins linearly from hub to tip.

Since 1984, the rotors of the hot high-pressure stages of industrial gas turbines have been made of GTD-111 DS (directional solidification) alloy metal and its successors, but these newer alloy metals are apparently also used in military aviation, because public information about their properties is very scarce compared to the old Nimonic alloys, which are 1960s technology. The GTD-111 DS blades probably can withstand about 800 °C without cooling. In that case, only the top two high-pressure stages would need cooling with 900 °C high temperate, and they could use internal cooling. The most recent public studies of turbine blade alloys are usually published by Chinese researchers [60]. Blades made of Lockheed Martin's MAR-M 200 DS (Directionally Solified) alloy seem to have better continuous tensile strength at 800 °C than Nimonic 105 alloy at 650 °C [61].

Since there is no free oxygen in the working fluid of the system, and the maximum bending stress is directed to the surface of the pressure side of the rotor, the blades of the very hot high-pressure stages could, at least in principle, be made of reinforced carbon-carbon composite[62]. Reinforced carbon-carbon is light and retain its strength up to 2000°C. However, the tensile strength of the graphite carbon spawn composites mentioned in the research literature has only been around 300 MPa [63]. The tensile strength of carbon fiber fibers is 900 GPa [64], so in principle, by adjusting the concentration and orientation of the carbon fiber, the greatest strength could be concentrated right on the pressure-side surface of the blade, but then the problem would be the insufficient compressive strength of the graphite composites on the opposite surface. Ti 6Al-4V carbon fiber composite is the most promising of the studied metal carbon fiber composites [65]and 5% carbon fiber content improves its tensile strength by more than 10%, but its maximum operating temperature 300 °C is too low. However, high temperature titanium matrix composites have better tensile strength and higher service temperature than conventional alloys [66].

Cryogenic compressor

The power of the cryogenic compressor is less than a fifth of the power of their hot counterparts with the same mass flow. Thus, the material technology places significantly fewer restrictions on its implementation. Below is an example implementation of an 11-stage 1:35.1 pressure ratio producing 62 MW refrigeration compressor. The mach number of the relative velocity of the gas flow at the blade front tip is kept at a constant value of 0.845. Mach number is relation velocity to speed of sound. Thus, the rotational velocity increases in the same

---

[60]https://www.researchgate.net/publication/370430660_Suppressing_temperature-dependent_embrittlement_in_high-strength_medium-entropy_alloy_via_hetero-grainprecipitation_engineering
[61]https://nickelinstitute.org/media/8d93486143182f5/nickel_incopub393_updated-june-2021.pdf
[62] https://en.wikipedia.org/wiki/Reinforced_carbon%E2%80%93carbon
[63]https://iccm-central.org/Proceedings/ICCM17proceedings/papers/D3.6%20Kobayashi.pdf
[64]https://www.frontiersin.org/journals/materials/articles/10.3389/fmats.2024.1374034/full
[65]https://www.mdpi.com/2504-477X/6/10/297
[66]https://core.ac.uk/download/pdf/333720346.pdf

proportion as the speed of sound, and the input power of the stages increases in proportion to the second power of the rotational velocity. Despite the increase in power, the hub/tip ratio can be kept at the optimal value of 0.65 for all stages. Below is an initial plan of a cryogenic compressor drawn by the simulation program and the detailed information of each stage.

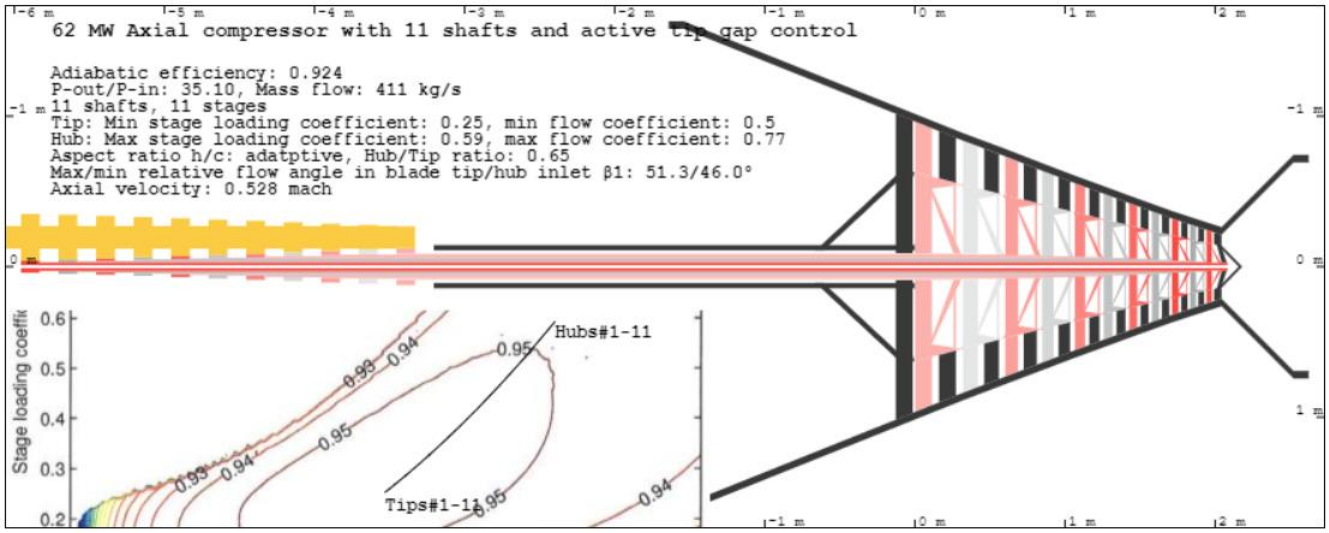

Figure 8. 11 axis and stage 62 MW refrigeration compressor

Cryogenic compressor	Pipe in	Stage 1	Stage 2	Stage 3	Stage 4	Stage 5	Stage 6	Stage 7	Stage 8	Stage 9	Stage 10	Stage 11	Pipe out
Temp K	76	73	79	87	96	106	116	128	142	156	172	190	222
P kPa	71	59	82	113	156	215	296	409	564	779	1071	1474	2509
Vx m/s	16	90	94	98	103	108	114	120	126	132	139	147	7
D mm	3156	1931	1676	1461	1274	1111	969	844	736	641	559	488	1384
h kJ/kg	76	72	80	88	96	106	117	129	142	156	172	189	220
P2/P1	0.82	1.39	1.38	1.38	1.38	1.38	1.38	1.38	1.38	1.37	1.38	1.38	1.23
Flow m3/s		146	114	91	73	58	46	37	29	23	19	15	
Power MW		3.4	3.6	4.0	4.4	4.8	5.3	5.9	6.5	7.2	8.0	8.9	
rpm		1793	2145	2580	3106	3740	4506	5434	6559	7935	9574	11579	
rTip mm		964	836	729	635	554	482	420	366	318	278	242	
Hub/Tip		0.65	0.65	0.65	0.65	0.65	0.65	0.65	0.65	0.65	0.65	0.65	
Blade h mm		337	293	255	222	194	169	147	128	111	97	85	
Chord mm		147	129	113	100	88	78	69	61	55	49	45	
Aspect ratio		2.29	2.27	2.25	2.23	2.20	2.17	2.13	2.09	2.03	1.97	1.90	
Mid flow t/h %		0.7	0.8	1.0	1.1	1.3	1.6	1.8	2.2	2.6	3.0	3.6	
Hub t/h %		1.3	1.5	1.8	2.1	2.5	2.9	3.5	4.1	4.8	5.7	6.7	
Re(c) EXP06		7.35	7.86	8.25	8.69	9.17	9.71	10.34	11.05	11.88	12.83	13.99	
Shaft radius mm		88	82	76	70	64	58	52	46	40	34	27	
Shaft torque %		33	34	36	39	43	49	56	67	82	83	81	
Shaft cent. stress %		0	1	1	1	1	1	1	1	2	2		
uShaft m/s		16.6	18.5	20.6	22.9	25.2	27.5	29.8	31.8	33.5	34.4	32.5	
uGear m/s		23.0	25.6	28.4	31.2	34.1	36.8	39.5	42.1	44.5	46.7	48.7	
Blades' load kN		27	28	30	31	33	34	36	38	40	42	44	
Shaft load kN		55	56	59	62	65	68	71	75	78	82	87	
Max blade stress MPa		350	350	350	350	350	350	350	350	350	350	350	
Centrifugal stress MPa		41	45	49	54	60	66	72	80	89	98	109	

The Reynolds numbers Re_c of the cryogenic compressor stages are about five times higher compared to the corresponding values of the main compressor. The difference is explained by the low kinematic viscosity of the cold gas. A high Reynolds number allows the aspect ratio to be increased somewhat from the above values, which would further reduce the losses of cryogenic turbomachines and improve the efficiency.

Energy storage building costs and profitability

The cost calculation of brand-new plants, processes, equipment, or work steps is always very uncertain. The most important thing is to carry out the work steps as far as possible with known cost-effective methods or by applying them and to use existing technology as far as possible. Most of the energy storage construction costs consist of large-scale open pit mining with large machines, crushing of rock material, compaction and strengthening of rock walls, and excavation of gas pipelines embedded in the wall. These unit costs are generally known, and the contract prices can therefore be easily calculated in advance. New work steps that are more difficult to evaluate are the pouring and masonry of distribution channels that can withstand the weight of the rock mass above, mixing of stone wool (or biochar) into a uniformly distributed gravel, construction of a moving gas tight layer between the storages, slowness and sealing of the gas tight stainless-steel plate surfaces of the above-ground part of the low-pressure storage, and construction and insulation of walls resistant to thermal movement of the above-ground part. Hot and cold gas pipelines and their control valves are standard process technologies. The total length of pipelines of different sizes is probably less than two kilometers.

Among the new work phases, the casting and masonry of vault structures and inclined wall structures are common construction techniques. The insulation layers can be made by alternately spreading equal-sized gravel and stone wool or biochar as a thin mat with trucks, and then harrowing them together. In the United States, the average price of biochar in 2023 was $131/ton [67], so on an industrial scale, the per ton price of biochar has settled somewhere between 100 and 200 euros. The specific weight of biochar is about 200 kg/m3. In this case, the price of one insulation cube would be less than 20 euros. It would be most advantageous to produce biochar in connection with a thermal power plant operating on wood or peat, where the gasifying half of the biomass would produce heat and electricity. The cost of cubic meter double density loose stone wool mixed with gravel would probably be less than 20 euros as well.

The size of the plant building is probably about the same as a simple gas turbine plant of similar power without heat recovery. The size of the hot compressors and turbines is significantly smaller because all the technology related to the combustion process and the synchronization with the generator is omitted. Vacuum gearboxes are quite small compared to electric power plant generators, so they would not take up significantly additional space either. The compressors and turbines on the cold side are also small.

The heat exchangers of the heat pump that freezes the cold gas would take up the most space, the total volume of which is estimated above to be around 2500 cubic meters and the supplier's stated list price with a temperature difference of two degrees is 10 million euros. With the default parameters, the size of the liquefied nitrogen expansion tank for a 2 TWh energy storage would be approximately 50,000 $m^{3.}$ It would fit in one cylinder-shaped tank made of austenitic steel partially buried in the ground, with an internal height and

[67] https://cloverly.com/ultimate-business-guide-to-biochar/#:~:text=Biochar%20price%3A%20The%20average%20biochar,their%20portfolio%20of%20carbon%20credits.

width of 40 meters. The partially underground insulation of the tank could be done, for example, with Röchlingin, which is used in the insulation of LNG tankers and tanks With Lignostone insulation [68]. The lowest operating temperature stated by its manufacturer is -196 °C.

If this pumped thermal energy storage concept out to be technically and economically feasible, it will at least be a new market area worth several billions for the existing manufacturers of turbines and compressors. It would likely allow rapid product development of turbomachines tailored to the concept, and perhaps also reasonable prices, as the first device supplier of a working prototype often has a clear commercial advantage in a new, rapidly expanding market segment.

The cost/MW of the turbine equipment of the power plant may already be lower for the prototype plant than for a simple gas turbine plant without heat recovery of same size, because the size and weight of its turbine and compressor equipment is probably only about 30-20% of the size of the corresponding equipment of the gas turbine plant.

The profitability of the investment depends on the plant's construction costs, operating costs, electricity price fluctuations and the total amount of electricity sold each year. The previous three years have been exceptionally turbulent in the electricity markets of Finland and the Nordic countries, but based on futures, the price fluctuations would be leveling off at least for the time being. In the long term, however, the trend seems to be the opposite, as the constant rise in the price of emission rights removes plants using fossil energy from the market, while the share of electricity production dependent on the sun and wind is constantly increasing. Thus, it can be assumed that in the longer term the turbulence will continue, and thus the need for adjustable electricity production will continue to grow. If the tax-free purchase price of the plant's electricity had been at most 2.5 cents/kWh and the selling price at least 3/kWh cents, then during the previous year the average margin would probably have been at least 5 cents/kWh and the total annual sale of electricity perhaps around 4 TWh. In that case, the facility's gross margin would have been over EUR 200 million. If the degree of automation is reasonable high, the annual operating and maintenance costs of the plant could be around 10–20 million euros, in which case the annual return on the investment would be at least 20% with the default parameters of the analysis program.

[68] https://www.roechling.com/fileadmin/downloads/Roechling_Industrial/Brochures/EN/Durolight/Cryogenic-insulation_materials-EN.pdf

Testing the concept

For the time being, this plan is based solely on public written sources, so the proposals and preliminary estimates presented above must be verified either by simulation or laboratory measurements.

The most important things to be verified are:

1. Feasibility study of proposed technical improvements of turbomachinery and calculation of their efficiencies using CFD modeling. The modeling should be fully parameterized to find the optimum in terms of unit power, efficiency, and cost.
2. The behavior of the carbon-free mild steel and aluminum gravel used in the gas insulation of the high-pressure storage in the thermal movement of the gravel, operating temperatures, and pressure.
3. U-value, compressive strength, and gas permeability in convection of compacted 1:1 grave and stone wool or biochar insulation. The gravel must be completely uniform in size and at least 70 mm in diameter. When compacted, its porosity should be about 0.5.
4. Measuring the hydraulic conductivity, thermal expansion coefficient, and heat exchange efficiency of the gravel. Measuring internal heat leakage of the gravel caused by thermal radiation of the designed gravel mixtures of the upper and lower pressure storage. The heat exchange efficiency is measured using forced convection at the designed gas flow rate. The gravel must be pressurized to its actual area of use.
5. Simulation and measurement of the gradual compression, and long-term durability of the mafic gravel mixture of the high-pressure storage when the gravel temperature is changing between the min and max temperature and the thermal expansion is compressing the gravel.

An expert more familiar with turbine and compressor technology will probably be able to assess the feasibility of proposed improvements. Other points can be measured empirically, for example, in a decommissioned steam power plant's pressure boiler, the central part of which is filled with a gravel to be investigated and the edge parts are insulated with gravel and stone wool or biochar mix. Nitrogen gas, pressurized with a centrifugal or screw compressor and heated with possible additional resistors, is led to the upper part of the boiler. The lower part has an adjustable pressure equalizer and a return pipe to the compressor. The outer surface of the pressure boiler has a dense water-cooling pipeline inside the insulation. Based on its cooling power, the U-value of the gravel insulation can be calculated. The hydraulic conductivity and the heat exchange efficiency of the gravel mix can be measured from the pressure and temperature change of the gas in inlet and outlet.

The gravel inside the boiler can be compressed by from the bottom with an expanding chamber made of carbon-free steel, which is pressurized with another compressor to the several Mega Pascals. The economic simulation of dozens of heating and cooling cycles may require another thermal storage, where the hot and cold released from the measured storage can be stored. If there is a heat exchanger in between, the second storage does not even have to be pressurized, but it can be, for example, a gravel inside an austenitic steel plate welded into a tube insulated with stone wool and which is heated and cooled by air.

You can order crushed olivine gabbro stone from, for example, Luvia's sauna stone quarries, but the purity of the crushed stone and the sieving of planned gravel may require special arrangements. Biochar can be ordered in bulk and 1.6m3 large sacks. When procuring and testing biochar, it is important to find out the pore size that is relevant for insulating it from thermal radiation. Biochar produced at high temperature has the smallest pore size. The compressed density of the tested loose stone wool should be approximately 0.072.

Summary

This study is a concrete initial proposal for the realization of a PTES plant with a low-cost and high electricity recovery efficiency. The main innovations of this study are:

- Combining a closed two-way Brayton cycle with a massive thermal energy storage.
- Construction of thermal storage with very affordable open pit mining technology.
- Using ultramafic or mafic rock that is resistant to temperature fluctuations.
- Implementation of thermal insulation of the storage with mixed gravel and stone wool or gravel and biochar that can withstand the high pressure and temperature of the storage.
- The technical implementation of the pressure insulation of the storage with the thermal movement and compaction of the gravel with flexible carbon-free steel, aluminum gravel, technical rubber or bitumen can be used in the cooler edge part.
- Optimizing the high-pressure stages of the plant's turbomachinery to their upper limit with nested pipe shafts, so that the optimal velocity and geometry can be used in each stage. Adjustable moving pipe shafts enable active tip-clearance control and an optimal rotor hub and tip radius, even in high-pressure stages.

All points mentioned above have been found to be technically feasible through programmatic modeling and are estimated to be very inexpensive compared to other seasonal electricity storage methods. In the modeling, we have taken into account as truthfully as possible the properties of the materials found in other studies, the physical equations related to the modeling, the known technical limitations and the costs of the corresponding equipment and the work steps used.

Motor-generators of hundreds of megawatts and vacuum gearboxes customized to power plants are existing commercial technology that can be adapted to a PTES plant with minor modifications. In principle, the plant's control system would be a combination of the systems of gas power plants and pumped power plants, complemented by predictive control of the pressure ratio and active tip gap control.

If the electricity storage presented here proves to be technically feasible, and its preliminary price estimate is even approximately correct, its global effects would be revolutionary in the energy sector. Solar cells and wind power already produce at least several euro cents/kWh cheaper electricity compared to electricity production with fossil fuels. If the almost free electricity produced during their production peaks can be stored long-term with a margin of about 3–4 cents/kWh, then electricity production based on fossil energy will become unprofitable almost everywhere. In addition, affordable electricity all year round would accelerate the replacement of coal, gas, and oil heating with heat pumps. Together, these would make the realization of the global goal of carbon neutrality in 2050 completely possible. On a global level, economic considerations and political realities have determined the use of fossil fuels and the continuous growth of their carbon emissions in electricity production. The only viable way to abandon the use of fossil fuels is to make their use economically unprofitable.